universe

MDPI

Review

Hyperons in Finite and Infinite Nuclear Systems

Isaac Vidaña

Istituto Nazionale di Fisica Nucleare, Dipartimento di Fisica "Ettore Majorana", Università di Catania, Via Santa Sofia 64, I-95123 Catania, Italy; isaac.vidana@ct.infn.it

Abstract: In this work, we shortly review the role and properties of hyperons in finite and infinite nuclear systems such as hypernuclei and neutron stars. Particularly, we describe different production mechanisms of hypernuclei, discuss some aspects of their γ-ray spectroscopy and their weak decay modes, and give a few strokes on their theoretical description. We reexamine also the role played by hyperons on the properties of neutron and proto-neutron stars with a special emphasis on the well-known "hyperon puzzle", of which we discuss some of the solutions that have been proposed to tackle this problem. Finally, we review the role of hyperons on the cooling properties of newly born neutron stars and on the so-called r-mode instability.

Keywords: hyperons; hypernuclei; neutron stars

Citation: Vidaña, I. Hyperons in Finite and Infinite Nuclear Systems. *Universe* **2021**, *7*, 376. https://doi.org/10.3390/universe7100376

Academic Editors: David Blaschke, Konstantin Maslov, Elena Litvinova and Evgeni Kolomeitsev

Received: 6 September 2021
Accepted: 6 October 2021
Published: 9 October 2021

1. Introduction

The presence of strange baryons, commonly known as hyperons, in hypernuclei and neutron stars permits the study of baryon interactions from an enlarged perspective, and the extension of our present knowledge of conventional nuclear physics to the SU(3)-flavor sector [1]. Hypernuclei, bound systems composed of neutrons, protons and one or more hyperons, were first observed in 1952 by Danysz and Pniewski in a balloon-flown emulsion stack where a hyperfragment was discovered [2]. Pion and proton beam production in emulsions and later in ^{4}He bubble chambers, where single-Λ hypernuclei were identified from the weak decay of the Λ hyperon into a proton and a π^-, followed these initial cosmic-ray observations of hypernuclei. The advent of separated K^- beams, which permitted the realization of counter experiments, lead to more systematic investigations of hypernuclei. A considerable amount of hypernuclear features, such as, e.g., the small spin-orbit strength of the hyperon–nucleon (YN) interaction or the fact that the Λ essentially retains its identity inside the nucleus, were revealed by in-flight (K^-, π^-) counter experiments carried out at CERN and at Brookhaven National Laboratory (BNL). Experiments using (π^+, K^+) and $(K^-_{stopped}, \pi^0)$ reactions were conducted later at the Brookhaven AGS and KEK accelerators with higher intensities and improved energy resolution of the beams. A high-precision tool for the study of Λ-hypernuclear spectroscopy with resolutions of several hundred keV [3] is provided by the electromagnetic production of hypernuclei through the reaction $(e, e'K^+)$ carried out at the Thomas Jefferson National Laboratory (JLAB) and the Mainz Microtron Accelerator (MAMI-C). A promising new way to produce hypernuclei by using stable and unstable heavy-ion beams was proposed a few years ago by the HypHI Collaboration at FAIR/GSI [4], and it has recently allowed the observation of the Λ hyperon, and the ${}^3_\Lambda$H and ${}^4_\Lambda$H hypernuclei in a first experiment using a ^{6}Li beam on a ^{12}C target at 2 AGeV [5]. Today, thanks to the use of high-energy accelerators and modern electronic counters, more than 40 single-Λ hypernuclei, and a few double-Λ and single-Ξ ones have been identified. The existence of single-Σ hypernuclei, however, has not been experimentally confirmed yet without ambiguity, suggesting that the ΣN interaction is most likely repulsive.

In addition to hypernuclei, a big interest has being put in the study of hyperonic matter (nuclear matter with nucleonic and hyperonic degrees of freedom), especially in connection with the physics of neutron star interiors [6–10]. The density in the interior of neutron

stars is large enough to allow for the appearance of new particles with strangeness content besides the conventional nucleons and leptons by means of weak interaction processes. Hyperons are expected to appear in neutron stars at around twice normal nuclear matter saturation density $\rho_0 = 0.16$ fm^{-3}. Neutron star properties are closely related to the underlying Equation of State (EoS) of matter at high densities. Therefore, despite the fact that hypernuclear matter is an idealized system, the theoretical determination of its EoS is an essential step towards the understanding of those neutron star properties which can be affected by the presence of hyperons. It is well known that the presence of hyperons softens the EoS and reduces the mass of neutron stars (see, e.g., [8,9]). In addition, hyperons can strongly influence also the thermal evolution and gravitational instabilities of these objects. The presence of hyperons, for instance, can modify the neutrino emissivity of dense matter and it can allow also for additional cooling mechanisms. Furthermore, hyperons dominate the bulk viscosity of matter as soon as they appear in the neutron star interior. Consequently, the emission of gravitational waves in hot and rapidly rotating neutron stars due to the so-called r-mode instability is affected also by their presence. Conversely, further constraints on the YN and hyperon–hyperon (YY) interactions can be provided by comparing the theoretical predictions for these properties with astrophysical observations.

A detailed knowledge of the EoS of hypernuclear matter over a wide range of densities is required to understand better the effect of hyperons on neutron stars. However, this is a very hard task. Two types of approaches have been traditionally used to describe baryon interactions in the nuclear medium and, to construct from them the (hyper)nuclear EoS: phenomenological and microscopic approaches. Relativistic or non-relativistic phenomenological approaches are based on effective density-dependent interactions which contain typically a certain number of parameters that are adjusted to reproduce (hyper)nuclear observables, and neutron star properties. Among the most commonly used ones, we can mention Skyrme-type interaction models and relativistic mean field (RMF) models. Several authors have used density-dependent baryon–baryon interactions based on Skyrme-type forces including hyperons to derive phenomenological EoSs of hyperonic matter [11–21]. Properties of nuclei and the experimental data from hypernuclei are employed within this approach to fix the in-medium nucleon–nucleon (NN), YN and YY interactions. RMF models are based on effective Lagrangian densities in which baryon–baryon interactions are described in terms of meson exchanges. A RMF description of the EoS of dense matter with hyperons is turning out today to be one of the most popular ones (see, e.g., [22–27]). The parameters of RMF models are usually determined by using, in the case of the nucleons, the properties of nuclei and nuclear bulk matter, and by employing symmetry relations and hypernuclear observables to fix the coupling constants of the hyperons with the mesons. The Quark-Meson-Coupling (QMC) model has also been employed to determine the EoS of (hyper)nuclear matter and the properties of neutron stars [28–36]. In the QMC model, baryons are treated as confined non-overlapping bags of three quarks where the interaction is modeled through the exchange of mesons between quarks from different bags, which are, in turn, modeled using the MIT bag model. The in-medium properties of hyperons have been also studied within the Non Linear Derivative (NLD) model, an alternative RMF approach which incorporates an explicit momentum dependence of the in-medium baryon optical potentials [37–39]. Microscopic approaches, on the other hand, are based on realistic two-body baryon–baryon interactions that describe the scattering data in free space. These interactions have been mainly constructed within the framework of the meson-exchange theory [40–50], although a new approach based on chiral perturbation theory has recently emerged as a powerful tool [51–59]. To obtain the EoS, one has to solve then the very complicated many-body problem. The main difficulty of this problem lies in the treatment of the repulsive core which dominates the short-range behavior of the baryon interaction. Different microscopic many-body methods have been extensively used to study nuclear matter, however, very few of them have been extended to the hypernuclear sector. To the best of our knowledge, the many-body methods extended to the strange sector include the Brueckner–Hartree–Fock (BHF) approximation [60–67] of the Brueckner–

Bethe–Goldstone theory, the Hartree–Fock theory based on the soft $V_{low\,k}$ interactions [68] and the Dirac–Brueckner–Hartree–Fock (BHF) theory [69]. The Auxiliary Field Diffusion Monte Carlo method [70] was also extended to the hyperonic sector a few years ago. Very recently BHF calculations of hyperonic matter using YN interactions derived within SU(3) chiral effective field theory have also been done by the Jülich–Bonn–Munich group [71,72] and Kohno [73,74].

This work is not intended to be an exhaustive review but rather a short introduction to the several aspects of hypernuclear physics. Here, we briefly review the properties of hyperons in hypernuclei and neutron stars. Particularly, in Section 2, we shortly discuss different production mechanisms of hypernuclei, as well as some aspects of their γ-ray spectroscopy, their weak decay modes, and their theoretical description. In Section 3, we reexamine the role played by hyperons on the properties of neutron and proto-neutron stars with a special emphasis on the so-called "hyperon puzzle" and present some of the possible solutions that have been proposed to tackle it. We also reexamine in this section the effect of hyperons on the cooling properties of newly born neutron stars and on the development of the so-called r-mode instability. The manuscript is finished in Section 4 with a summary.

2. Hypernuclear Physics in a Nutshell

Compared to the NN interaction, the YN and YY ones are still poorly constrained due, mainly, to the scarce amount of YN scattering data and to the complete absence of them in the YY case. The reason of this scarce amount of data should be traced back to the experimental difficulties associated with the short lifetime of hyperons and the low-beam intensity fluxes. In addition to the scattering data, information on the YN and YY interactions can be obtained, using the so-called femtoscopy technique, by measuring the correlations (in momentum space) of Yp and YY pairs produced in heavy-ion collisions [75–85]. The ratio of the distribution of relative momenta $\vec{k}^* = (\vec{p}_1 - \vec{p}_2)/2$ between a correlated and uncorrelated pair defines the correlation function of a given baryon pair. If the interaction of a baryon pair is attractive, then the measured correlation function will be found to be larger than one. Conversely, if the interaction of the pair is repulsive, the correlation function will take values between zero and one. The correlation function between two baryons can be theoretically expressed as [86,87]

$$C(\vec{k}^*) = \int d^3\vec{r} |\psi(\vec{k}^*, \vec{r})|^2 S(\vec{r}) \,, \tag{1}$$

where $\psi(\vec{k}^*, \vec{r})$ is the relative wave function of the baryon pair of interest and $S(\vec{r})$ is the so-called source function, and it represents the distribution of the distance $|\vec{r}|$ at which the particles are emitted. The comparison between the theoretical correlation function and the measured one permits the testing and improvement of the existing YN and YY potentials.

Lattice QCD offers also a very powerful way to derive baryon–baryon interactions, see, e.g., [88–93] for reviews. A big progress in this direction has been made in the last years by the HALQCD [94–102] and the NPLQCD [103–105] collaborations. We should note, however, that the methods employed by these two collaborations are quite different. Whereas the HALQCD collaboration follows a method to extract the different baryon–baryon potentials from the Nambu–Bethe–Salpeter wave function measured on the lattice, the NPLQCD collaboration combines calculations of correlation functions at several light-quark-mass values with low-energy effective field theory (EFT). This second approach is particularly interesting because it allows the matching of lattice QCD results with low-energy EFT providing, in this way, the means for first predictions in the physical quark mass limit. Results for various NN, NY and YY interaction channels at a single value of the lattice spacing and of the lattice volume have been recently obtained by the HALQCD collaboration which managed to approach the region of physical masses [100–102]. Very recently, the NPLQCD collaboration has studied the interaction between two octet baryons for strangeness $S = 0, -1, -2, -3$ and -4 at low energies using larger-than-physical quark

masses corresponding to a pion mass of $m_\pi \sim 450$ MeV and a kaon mass of $m_K \sim 596$ MeV, and have extracted the corresponding values of s-wave scattering phase shifts, low-energy scattering parameters, and binding energies of two-baryon bound systems [105]. A detailed review of the last lattice QCD developments in the strangeness sector is beyond the scope of the present paper and, therefore, the interested reader is referred to the original works of both the HALQCD and the NPLQCD collaborations for further information.

Alternative and complementary information on the YN and YY interactions can be extracted from the study of hypernuclei. The main aim of hypernuclear physics [106,107] is, in fact, to relate hypernuclear observables with the underlying YN and YY interactions. In this section, we briefly review the different production mechanisms of hypernuclei, discuss some aspects of their γ-ray spectroscopy and their weak decay modes, and we finish with a few strokes on their theoretical description.

2.1. Production of Hypernuclei

Several reactions can be used to produce single-Λ hypernuclei. One of them is the so-called (K^-, π^-) *strangeness exchange reaction*

$$K^- + {}^A Z \rightarrow {}^A_\Lambda Z + \pi^- \,, \tag{2}$$

where a neutron of the nucleus target hit by a K^- is changed into a Λ that remains bound to the nucleus and a π^- is emitted. With this reaction, it is possible to determine accurately the mass and the binding energy of the formed hypernucleus by measuring the momenta of both the incoming K^- and the outgoing π^- using two magnetic spectrometers with good energy resolution. Strangeness exchange reactions, initially performed at CERN, have been mainly used later at BNL in the USA, and at KEK and J-PARC in Japan.

The so-called (π^+, K^+) *associated production reaction* is another production mechanism of hypernuclei that makes use of π^+ beams instead of K^- ones,

$$\pi^+ + {}^A Z \rightarrow {}^A_\Lambda Z + K^+ \,. \tag{3}$$

Here, an $s\bar{s}$ pair is created from the vacuum, and a K^+ and a Λ are produced in the final state. The production cross section of this reaction is smaller than that of the (K^-, π^-) one, but this is compensated by the fact that the intensities of the π^+ beams are larger than those of the K^- ones. The production of hypernuclei by means of these reactions have been also performed at BNL and KEK, and later at GSI in Germany.

The use of electron beams with an excellent spatial and energy resolution has allowed the *electroproduction* of hypernuclei by means of the $(e, e'K^+)$ reaction,

$$e^- + {}^A Z \rightarrow e^- + K^+ + {}^A_\Lambda (Z-1) \,, \tag{4}$$

providing in addition a high-precision tool for the study of hypernuclear spectroscopy, with energy resolutions of several hundred keV [3]. Electroproduction of hypernuclei is carried out at JLAB in the USA and the MAMI-C laboratory in Germany. These two laboratories are presently the only ones with the instrumental capabilities required to perform these kind of experiments.

The kinematics of the elementary processes $n(K^-, \pi^-)\Lambda$, $n(\pi^+, K^+)\Lambda$ and $p(\gamma, K^+)\Lambda$ underlying the three production mechanisms of single Λ-hypernuclei discussed above is shown in Figure 1, adapted from [108]. Note that the momentum transferred to the Λ is much lower in the case of the $n(K^-, \pi^-)\Lambda$ reaction than in the other two. The lower the momentum transferred to the Λ is, the larger its probability of interacting with, or being bound to, the nucleus will be. In addition, the lower the momentum transferred is, the smaller the angular momentum transfer will also be and, consequently, the Λ will more easily retain the quantum numbers of the nucleon that has been eliminated in the reaction. Therefore, in the case of the $n(\pi^+, K^+)\Lambda$ or $p(\gamma, K^+)\Lambda$ reactions, since the recoil

momentum of the hyperon is high, the cross sections to bound states are reduced, and the produced Λ has a higher probability of escaping the nucleus.

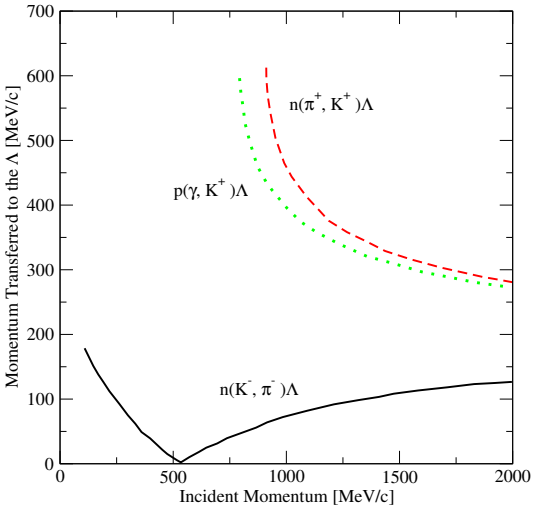

Figure 1. Momentum transferred to the Λ as a function of the incident particle momentum for the elementary process $n(K^-, \pi^-)\Lambda$, $n(\pi^+, K^+)\Lambda$ and $p(\gamma, K^+)\Lambda$ at 0^0. Figure adapted from [108].

Similar reactions can be used to produce single-Σ hypernuclei. However, as we have already said, their existence has not been yet experimentally confirmed without ambiguity. The production of double-Λ hypernuclei requires a two-step mechanism in which, first, a Ξ^- is created by means of reactions such as

$$\bar{p} + p \rightarrow \Xi^- + \bar{\Xi}^+ \tag{5}$$

or

$$K^- + p \rightarrow \Xi^- + K^+ , \tag{6}$$

and second, the Ξ^- is captured in an atomic orbit and interacts with the nuclear core, producing two Λ's by hitting one of the protons of the nuclei

$$\Xi^- + p \rightarrow \Lambda + \Lambda . \tag{7}$$

This process releases an energy of about 30 MeV that, in most of the cases, is equally shared between the two Λ's, leading to the escape of one or both hyperons from the nucleus.

Double-Λ hypernuclei are currently the best systems to investigate the properties of the baryon–baryon interaction in the strangeness $S = -2$ sector. The ΛΛ bond energy $\Delta B_{\Lambda\Lambda}$ in double-Λ hypernuclei can be experimentally determined by measuring of the binding energies of double and single-Λ hypernuclei as

$$\Delta B_{\Lambda\Lambda} = B_{\Lambda\Lambda}({}^{A}_{\Lambda\Lambda}Z) - 2B_{\Lambda}({}^{A-1}_{\Lambda}Z) . \tag{8}$$

A few double-Λ hypernuclei, ${}^{6}_{\Lambda\Lambda}$He, ${}^{10}_{\Lambda\Lambda}$Be and ${}^{13}_{\Lambda\Lambda}$B, have been reported in emulsion experiments. A quite large value of the ΛΛ bond energy of around 4 to 5 MeV was deduced from the subsequent analysis of these emulsion experiments. We should also note that the identification of some of these double-Λ hypernuclei was ambiguous. Therefore, careful attention should be paid when using the data from this old analysis to put any kind of constraint on the ΛΛ interaction. However, a new ${}^{6}_{\Lambda\Lambda}$He candidate with a ΛΛ bound energy $\Delta B_{\Lambda\Lambda} = 1.01 \pm 0.2^{+0.18}_{-0.11}$ MeV (recently corrected to $\Delta B_{\Lambda\Lambda} = 0.67 \pm 0.17$ MeV) was observed without ambiguity in 2001 at KEK [109].

The reactions (5) and (6) can be used to produce single-Ξ hypernuclei and, in fact, a few of them have been identified. The analysis of the experimental data from reactions such as ${}^{12}\mathrm{C}(K^-, K^+){}^{12}_{\Xi^-}$Be [110] indicates an attractive Ξ-nucleus interaction of ~ -14 MeV.

Recently, however, Friedman and Gal [111] have analyzed several $\Xi^- p \to \Lambda\Lambda$ two-body capture events in ^{12}C and ^{14}Ni emulsion nuclei, concluding that the Ξ-nuclear interaction is strongly attractive, with a Ξ^- potential depth in nuclear matter $V_{\Xi^-} \geq 20$ MeV. We should mention here the observation [112] of a deeply bound state of the Ξ^--^{14}N system with a binding energy of 3.87 ± 0.21 MeV [113]. This event provides the first clear evidence of a deeply bound state of this system by an attractive ΞN interaction. The latest experimental data obtained by the J-PARC E07 collaboration [114] indicate a value for the binding energy of the Ξ^- in the Ξ^--^{14}N system of 1.27 ± 0.21 MeV. Future Ξ hypernuclei experiments are being planned at J-PARC.

2.2. γ-ray Spectroscopy of Hypernuclei

Excited states of hypernuclei can be produced when a nucleon in a p or a higher shell is replaced by a hyperon. The energy of the hypernuclear excited states can be released either by emitting nucleons or, sometimes, γ-rays. The analysis of hypernuclear excited states with very good energy resolution has been possible thanks to the detection of γ-ray transitions in single-Λ hypernuclei. The construction of large-acceptance germanium detectors, dedicated to hypernuclear γ-ray spectroscopy, has overcome some of the initial technical difficulties found in the application of γ-ray spectroscopy to hypernuclei. These difficulties were mostly associated with the detection efficiency of γ-ray measurements and with the necessity of covering a large solid angle with γ-ray detectors. Several weak points in hypernuclear γ-ray spectroscopy, however, still persist such as, for instance, the fact that the observation of γ-rays is mostly limited to the low excitation region, maybe up to the Λ p-shell. The reason is that a number of single-particle Λ states are bound in heavy Λ hypernuclei with a potential depth of ∼28 MeV but the energy levels of many single-particle states are above the neutron and proton emission thresholds. Another weak point is clearly the fact that the γ-ray transition only measures the energy difference between two states and this single energy information is not enough to fully identify the two levels. This problem can be solved, of course, by measuring two γ-rays in coincidence. We show in Figure 2 the energy of a Λ hyperon in the single-particle states s, p, d, f and g of several hypernuclei, deduced from emulsion, (K^-, π^-) and (π^+, K^+) reactions, as a function of the mass number to the power $-2/3$. The value of ∼28 MeV extrapolated at $A^{-2/3} = 0$ is usually interpreted as the binding energy of a single Λ hyperon in infinite symmetric nuclear matter at saturation density, and it is used to fix the parameters of the majority of the models of the hyperonic EoS. Systematic spectroscopic studies of single Λ hypernuclei indicate that the ΛN interaction is attractive [115].

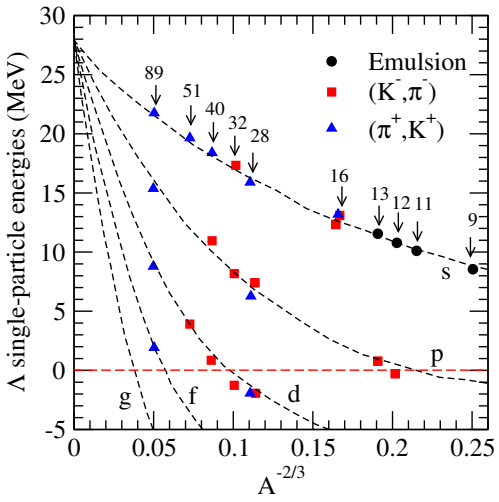

Figure 2. Energy of a Λ hyperon in the single-particle states s, p, d, f and g of several hypernuclei as a function of $A^{-2/3}$ deduced from emulsion, (K^-, π^-) and (π^+, K^+) reactions. The lines are drawn just to help the reader.

To finish this section, in Figure 3, we show, as an example, the level scheme and γ-ray transitions of ${}^{16}_{\Lambda}$O identified and determined by γ-ray spectroscopy using the (K^-, π^-) reaction and the germanium detector array *Hyperball* at BNL [116]. The twin peaks observed confirm the hypernuclear fine structure for the $(1^- \rightarrow 1^-)$ and $(1^- \rightarrow 0^-)$ transitions in ${}^{16}_{\Lambda}$O. We note that the small spacing between the twin peaks is due to the spin dependence of the ΛN interaction.

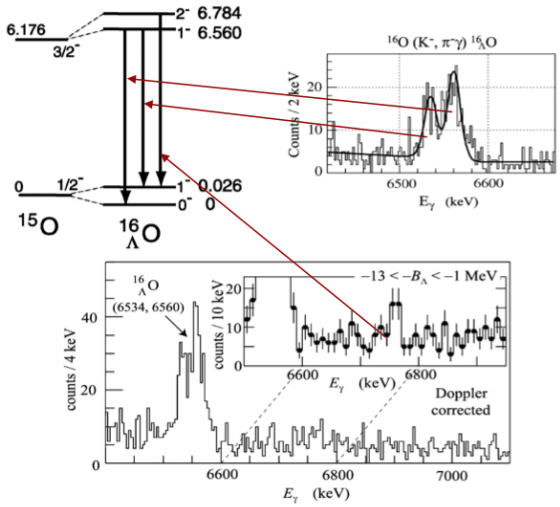

Figure 3. Level scheme and γ-ray transitions and ${}^{16}_{\Lambda}$O measured at BNL. Figure adapted from [116].

2.3. Weak Decay of Hypernuclei

The so-called mesonic weak decay

$$\Lambda \rightarrow N + \pi\,, \quad p_N \sim 100 \text{ MeV/c} \tag{9}$$

is the main decay mode of the Λ hyperon in free space, where $\sim$60% of the times the Λ decays into a proton and a π^-, and $\sim$40% into a neutron and a π^0. When the Λ is bound in the nucleus, however, this mode is strongly suppressed by the Pauli exclusion principle since the momentum of the outgoing nucleon ($\sim$100 MeV/c) is smaller than the typical Fermi momentum of a nucleon in the nucleus ($\sim$270 MeV/c). Consequently, in hypernuclei (specially in medium and heavy ones), the dominant decay mode becomes the non-mesonic one

$$\Lambda + N \rightarrow N + N\,, \quad p_N \sim 420 \text{ MeV/c} \tag{10}$$

$$\Lambda + N + N \rightarrow N + N + N\,, \quad p_N \sim 340 \text{ MeV/c} \tag{11}$$

where the Λ interacts with one (or more) of the surrounding nucleons. The weak decay of hypernuclei has been mainly studied within the framework of meson-exchange models [117,118] and, more recently, using the effective field theory [119,120]. In [121,122], the interested reader can find two comprehensive reviews on the theoretical aspects of hypernuclear weak decay.

In Figure 4, we present the weak decay rate Γ (expressed in units of the decay rate of the Λ in free space) as function of the total number of particles $A + 1$. The figure has been adapted from the original one in [123]. The dot, dashed and solid lines show, respectively, the theoretical predictions of the mesonic Γ_M, non-mesonic Γ_{NM} and total Γ_T decay rates. The curves labeled Γ_1 and Γ_2 correspond to the contributions of one-nucleon and two-nucleon induced decay modes to the non-mesonic decay rate (see Equations (10) and (11)). Experimental values of the total and non-mesonic decay rates are given, respectively, by the squares and circle marks. As it can be seen in the figure, the mesonic decay mode gets blocked as A increases, while the non-mesonic decay increases up to a saturation

value of the order of the free decay, reflecting the short-range nature of the weak $\Delta S = 1$ baryon–baryon interaction.

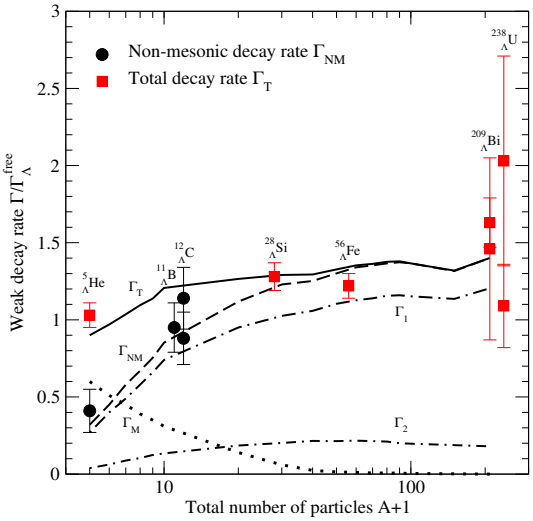

Figure 4. Weak decay rate Γ as a function of the total number of particles in units of the weak decay rate of the Λ in free space $\Gamma_\Lambda^{\text{free}}$. Dot, dashed and solid lines show, respectively, the theoretical predictions of the mesonic Γ_M, non-mesonic Γ_{NM} and total Γ_T decay rates. Dot-dashed lines labeled Γ_1 and Γ_2 display the contributions of one-nucleon and two-nucleon induced decay modes to the non-mesonic decay rate (see Equations (10) and (11)). Experimental values of the total and non-mesonic decay rates are given by the squares and circle marks, respectively. Figure adapted from the original one in [123].

2.4. Theoretical Description of Hypernuclei

A simple theoretical description of a hypernucleus consists of an ordinary nucleus with a hyperon sitting in a single particle state of an effective hyperon-nucleus mean field potential. Based on this simple description, several approaches have been followed to derive the properties of hyperons in finite nuclei. Traditionally, Woods–Saxon potentials have been used, for instance, to describe in a shell model picture the single-particle properties of the Λ from medium to heavy hypernuclei [124–127]. To improve the overall fit of the Λ single-particle energies, non-localities and density-dependent effects have been included in non-relativistic Hartree–Fock calculations with Skyrme type YN interactions [13–21]. Relativistic mean field theory [24,128–137] and Dirac phenomenology [138,139] have been also employed to perform hypernuclear structure calculations. Several hypernuclear structure studies based on ab initio approaches do also exist in the literature [140–147]. The single-particle properties of the Λ in the hypernucleus are derived in these studies from effective YN G-matrices built from bare YN interactions which describe the scarce scattering data in free space. A Quantum Monte Carlo calculation of single- and double-Λ hypernuclei has also been recently done using two- and three-body forces between the Λ and the nucleons [70,148]. We would like to note that the NPLQCD collaboration has been able to obtain the binding energies of the light hypernuclei including ${}^{3}_{\Lambda}$He, ${}^{4}_{\Lambda}$H and ${}^{4}_{\Lambda\Lambda}$He [149].

The quality of the description of hypernuclei in most of these approaches relies on the validity of the mean field picture. Correlations induced by the YN interaction can, however, change substantially this picture and, therefore, should not be ignored. While many authors have extensively studied the correlations of nucleons in nuclear matter and finite nuclei, those of hyperons have not received so much attention so far. The effect of the Λ correlations in nuclear matter, beyond the mean field description, was studied for the fist time by Robertson and Dickhoff [150] using the Green's function formalism. These authors calculated the spectral function and quasi-particle parameters of the Λ finding

results qualitatively similar to those of the nucleons. They showed that the Λ is, in general, less correlated than the nucleons. A few years ago, the author of the present review studied the spectral function of the Λ hyperon in finite nuclei [151], showing, in agreement with the work of Robertson and Dickhoff, that the Λ is less correlated than the nucleons, and confirming the idea that it maintains its identity inside the nucleus. The results of this study showed also that in hypernuclear production reactions, the Λ hyperon is formed mostly in a quasi-free state.

As an example of a theoretical calculation of hypernuclei, we briefly describe here a microscopic method that allows one to determine the single-particle bound states of a Λ-hyperon in finite nuclei. This method starts with the construction of all the YN G-matrices which describe the interaction between a hyperon and a nucleon in infinite nuclear matter. To this end, the coupled-channel Bethe–Goldstone equation is solved. These G-matrices are then used to obtain the YN G-matrices in finite nuclei through the following integral equation:

$$\begin{aligned} G_{FN} &= G + G\left[\left(\frac{Q}{E}\right)_{FN} - \left(\frac{Q}{E}\right)\right] G_{FN} \\ &= G + G\left[\left(\frac{Q}{E}\right)_{FN} - \left(\frac{Q}{E}\right)\right] G \\ &+ G\left[\left(\frac{Q}{E}\right)_{FN} - \left(\frac{Q}{E}\right)\right] G\left[\left(\frac{Q}{E}\right)_{FN} - \left(\frac{Q}{E}\right)\right] G \\ &+ \cdots, \end{aligned} \tag{12}$$

which expresses the finite nuclei G-matrices, G_{FN} , in terms of the nuclear matter ones, G, and the difference between the finite-nucleus and the nuclear-matter propagators, written schematically as $(Q/E)_{FN} - (Q/E)$. This difference, which accounts for the relevant intermediate particle–particle states has been shown to be quite small and, thus, in all practical calculations, G_{FN} can be well approximated by truncating the expansion of Equation (12) up to second order in the nuclear matter G-matrices. Therefore, we have

$$G_{FN} \approx G + G\left[\left(\frac{Q}{E}\right)_{FN} - \left(\frac{Q}{E}\right)\right] G\,. \tag{13}$$

Using then G_{FN} as an effective YN interaction, one can obtain the Λ self-energy in the BHF approximation (see diagram (a) of Figure 5). This approximation can be split into the sum of two contributions: the one shown by diagram (b), which originates from the first-order term on the right-hand side of Equation (13), and that of diagram (c), which stands for the so-called two-particle-one-hole (2p1h) correction, where the intermediate particle–particle propagator has to be viewed as the difference of propagators appearing in Equation (13). Solving finally the Schrödinger equation with the real part of the Λ self-energy, it is then possible to determine, as mentioned before, the different Λ single-particle bound states. Further details of this method can be found, e.g., in [146,151].

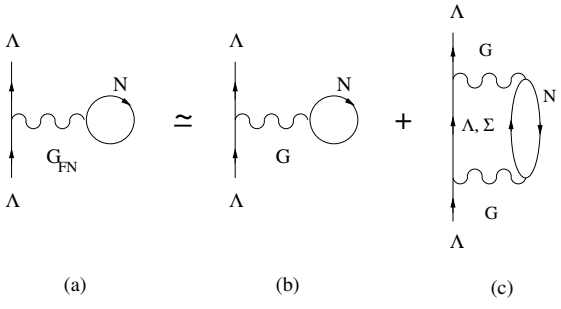

Figure 5. BHF approximation of the finite nucleus Λ self-energy (**a**), split into the sum of a first order contribution (**b**) and a second order 2p1h correction (**c**).

As an example of the application of this method, in Table 1, we show the energies of the Λ single-particle bound states in several hypernuclei. The results have been obtained with the NLO13 [58] and the NLO19 [59] chiral YN interaction of the Jülich–Bonn–Munich group for different values of the cutoff of the interaction including both contributions (first order term and 2p1h correction) to the Λ self-energy. We note that, due to technicalities of this method, it can be only applied to hypernuclei consisting of a closed-shell nuclear core plus a Λ sitting in a single-particle state. The values reported are to be compared with the experimental separation energies for the corresponding hypernuclei. However, since experimental data for the particular hypernuclei we consider do not always exist, the comparison is done with the closest representative hypernuclei for which experimental information is available. As it can be seen, in general, there is an underbinding of light hypernuclei such as ${}^{5}_{\Lambda}$He and ${}^{13}_{\Lambda}$C while the description of medium and heavy hypernuclei improves. Note, however, that neither the NLO13 interaction nor the NLO19 one yield a quantitative description of all medium and heavy hypernuclei. Whereas the NLO19 interaction describes reasonably well ${}^{17}_{\Lambda}$O, ${}^{41}_{\Lambda}$Ca and ${}^{91}_{\Lambda}$Zr, it seems to overbind ${}^{209}_{\Lambda}$Pb. For the latter, the predictions of the NLO13 interaction are more in line with the experiment. We note that the results of the calculation agree with the experimental fact that the spin-orbit splitting of the *p*-, *d*-, *f*- and *g*-states is very small. The interested reader is referred to [147] for further detail of these results.

Table 1. Energy of the Λ single-particle bound states for several hypernuclei from ${}^{5}_{\Lambda}$He to ${}^{209}_{\Lambda}$Pb. Results are shown for the chiral *YN* interactions NLO13 [58] and NLO19 [59] of the Jülich–Bonn–Munich group for different values of the cutoff of the interaction. Available experimental data [107,152] for the closest measured hypernuclei are included. † The weak signal for ${}^{40}_{\Lambda}$Ca [153] is not included in the recent compilation in [107].

	NLO13					NLO19					Exp.
Cutoff (MeV)	**500**	**550**	**600**	**650**	**700**	**500**	**550**	**600**	**650**	**700**	
${}^{5}_{\Lambda}$He											${}^{5}_{\Lambda}$He
$s_{1/2}$	−0.73	−0.15	−0.63	−2.36	−4.90	−2.16	−1.36	−1.77	−3.42	−5.63	−3.12(2)
${}^{13}_{\Lambda}$C											${}^{13}_{\Lambda}$C
$s_{1/2}$	−4.44	−2.24	−3.72	−8.91	−13.40	−8.91	−6.42	−7.22	−10.81	−14.98	−11.69(12)
$p_{3/2}$	–	–	–	–	−1.22	–	–	–	−0.12	−1.76	−0.8(3) (p)
$p_{1/2}$	–	–	–	–	−0.97	–	–	–	–	−1.40	
${}^{17}_{\Lambda}$O											${}^{16}_{\Lambda}$O
$s_{1/2}$	−6.07	−3.46	−5.35	−10.51	−16.37	−11.46	−8.61	−9.55	−13.60	−18.18	−13.0(2)
$p_{3/2}$	–	–	–	−1.22	−4.04	−1.26	−0.14	−0.53	−2.40	−4.89	−2.5(2) (p)
$p_{1/2}$	–	–	–	−0.66	−3.31	−0.51	–	–	−1.69	−4.10	
${}^{41}_{\Lambda}$Ca											${}^{40}_{\Lambda}$Ca
$s_{1/2}$	−12.37	−8.78	−11.24	−17.56	−24.36	−19.51	−15.86	−16.80	−21.30	−26.47	−18.7(1.1) †
$p_{3/2}$	−4.95	−2.54	−3.98	−8.82	−13.43	−9.91	−6.93	−7.48	−11.04	−15.06	−11.0(5) (p)
$p_{1/2}$	−4.37	−2.08	−3.50	−7.73	−12.87	−9.13	−6.23	−6.82	−10.42	−14.47	
$d_{5/2}$	–	–	–	−0.40	−3.59	−1.47	–	–	−1.99	−4.67	−1.0(5) (d)
$d_{3/2}$	–	–	–	−0.50	−4.02	−0.56	–	–	−1.20	−3.84	
${}^{91}_{\Lambda}$Zr											${}^{89}_{\Lambda}$Y
$s_{1/2}$	−19.36	−14.66	−17.83	−25.10	−32.50	−27.72	−22.57	−23.19	−28.94	−34.61	−23.6(5)
$p_{3/2}$	−14.24	−10.59	−13.27	−19.27	−25.45	−20.59	−16.24	−16.94	−22.05	−26.96	17.7(6) (p)
$p_{1/2}$	−13.95	−10.39	−13.05	−19.07	−25.31	−20.45	−15.96	−16.67	−21.86	−26.82	
$d_{5/2}$	−6.21	−3.33	−5.24	−10.30	−15.27	−11.92	−8.10	−8.44	−12.68	−16.78	−10.9(6) (d)
$d_{3/2}$	−5.80	−2.98	−4.88	−9.70	−14.97	−11.65	−7.61	−7.98	−12.27	−16.40	
$f_{7/2}$	–	–	–	−1.68	−5.63	−4.04	−0.98	−0.89	−3.97	−7.04	−3.7(6) (f)
$f_{5/2}$	–	–	–	−1.28	−5.23	−3.59	−0.33	−0.28	3.39	−6.54	
${}^{209}_{\Lambda}$Pb											${}^{208}_{\Lambda}$Pb
$s_{1/2}$	−25.75	−21.41	−25.09	−32.28	−39.51	−36.28	−29.50	−29.60	−35.84	−41.58	−26.9(8)
$p_{3/2}$	−21.88	−15.77	−18.33	−25.13	−31.83	−33.72	−26.73	−25.27	−30.26	−34.71	−22.5(6) (p)
$p_{1/2}$	−21.55	−15.53	−18.14	−25.00	−31.74	−33.58	−26.57	−25.13	−30.17	−34.64	
$d_{5/2}$	−14.47	−8.79	−9.96	−14.78	−19.98	−25.49	−19.28	−16.84	−20.08	−23.15	−17.4(7) (d)
$d_{3/2}$	−14.35	−8.71	−9.83	−14.62	−19.83	−25.29	−18.98	−16.57	−19.85	−22.97	
$f_{7/2}$	−4.46	–	–	−5.91	−12.57	−16.23	−10.15	−7.91	−11.90	−15.80	−12.3(6) (f)
$f_{5/2}$	−4.42	–	–	−5.60	−12.24	−15.96	−9.70	−7.47	−11.47	−15.38	
$g_{9/2}$	−1.87	–	–	−3.23	−9.21	−13.72	−7.55	−5.18	−8.92	−12.32	−7.2(6) (g)
$g_{7/2}$	−1.38	–	–	−2.91	−8.94	−13.38	−7.03	−4.69	−8.53	−12.00	

3. Hyperons and Neutron Stars

The presence of hyperons in the interior of neutron stars has been considered by many authors for more than 60 years since the seminal work of Ambartsumyan and Saakyan [154].

Different phenomenological or microscopic models have been used to describe the neutron star matter EoS. All the works show that hyperons may appear in the neutron star interior at densities around $2-3\rho_0$. The reason for their appearance is simply that, at such densities, the nucleon chemical potential is large enough to make the conversion of nucleons into hyperons energetically favorable. As a result of this conversion, the Fermi pressure exerted by nucleons is relieved and, therefore, the EoS becomes softer. Consequently, the mass of the star, and particularly, its maximum value M_{max} is reduced. How much the EoS is softened, and how much M_{max} is reduced depends on the attractive or repulsive character of the YN and YY interactions. In general, attractive (repulsive) interactions lead to an earlier (later) onset and larger (smaller) concentration of hyperons and, thus, to a stronger (more moderate) softening of the EoS and a larger (smaller) reduction of M_{max}. It is well known (see, e.g., [66,67]), however, that hyperons equalize the effect of different nucleonic interactions through several compensation mechanisms: a stiffer nucleonic EoS will lead to an earlier onset of hyperons enhancing in this way the softening due to their presence. Conversely, a retarded onset of a certain hyperon species will favor the appearance of other species leading also to a softer EoS. As a result, M_{max} is surprisingly quite insensitive to the pure nucleonic EoS, and even to the details of the YN and YY interactions (see, e.g., Figure 2 in [66] or Figure 3 in [67]).

3.1. The Hyperon Puzzle and Some Possible Solutions

Although the presence of hyperons in neutron stars seems to be energetically unavoidable, the strong softening of the EoS associated with the onset of hyperons (notably in microscopic models) leads to values of M_{max} not compatible with observations. This controversy is known in the literature as the "hyperon puzzle", and is currently a subject of intensive research. The discrepancy between the theory and observations became more dramatic after the measurements in the last decade of unusually high masses of the millisecond pulsars PSR J1903 + 0327 ($1.667 \pm 0.021 M_\odot$) [155], PSR J1614-2230 ($1.928 \pm 0.017 M_\odot$) [156], PSR J0348 + 0432 ($2.01 \pm 0.04 M_\odot$) [157], and the most massive one observed up to now PSR J0740 + 6620 ($M > 2.14^{+0.10}_{-0.09} M_\odot$) [158], which rule out almost all currently proposed EoS with hyperons (both microscopic and phenomenological).

To solve this puzzle, a mechanism (or mechanisms) is necessary that could provide the additional repulsion needed to make the EoS stiffer and, therefore, M_{max} compatible with the current observational limits. Three possible mechanisms that could provide such additional repulsion are: (i) more repulsive hyperon–hyperon interactions driven by either repulsive vector mesons exchanges [22,23,25–27] or less-attractive scalar σ meson exchange [24] (ii) repulsive hyperonic three-body forces [159–167] and (iii) a phase transition to deconfined quark matter at densities below the hyperon threshold [168–179]. The possible appearance of other hadronic degrees of freedom, such as the Δ isobar or meson condensates, that can push the onset of hyperons to higher densities, has been also considered. An interesting possibility to circumvent the problem is the so-called two-families scenario proposed in [180,181], in which stars made of hadrons are stable only up to $(1.5-1.6) M_\odot$ while most massive compact stars are entirely made of strange quark matter. In the following, we briefly review some of these possible solutions.

3.1.1. Hyperon–Hyperon Repulsion

This possible solution has been explored mostly in the context of RMF models [22–27], and it is based on the well-known fact that, in meson-exchange models of nuclear forces, while the scalar meson σ is responsible for the intermediate-range attraction, vector mesons generate repulsion at short distances. It has been argued that if the interaction between two hyperons, driven by vector mesons, is repulsive enough or the attraction mediated through the exchange of the σ meson is weak enough, then the EoS could be sufficiently stiff to reconcile the current high pulsar mass observations with the existence of hyperons in neutron stars. However, the strength of meson exchanges should be modified consistently with hypernuclear data which requires, at least, the ΛN interaction to be attractive and

suitably tuned to the hypernuclear data [115]. Such tuning is not required if the repulsive vector meson interactions act only among the hyperons through the exchange of the strange ϕ vector meson (which couples only to hyperons). In this way, the onset of hyperons is shifted to higher densities and it is possible to obtain neutron stars with maximum masses larger than $2M_{\odot}$ and a significant amount of hyperons in their interior.

3.1.2. Hyperonic Three-Body Forces

It is well known that three-nucleon forces are fundamental to reproduce accurately the properties of few-nucleon systems as well as the empirical saturation point of symmetric nuclear matter in non-relativistic many-body approaches. It seems natural, therefore, to suggest that three-body forces of the type NNY, NYY and YYY, involving one or more hyperons, could provide, as in the case of three-nucleon forces, the additional repulsion needed at high densities to make the EoS stiff enough, solving in this way the hyperon puzzle. This idea was suggested even before the observation of neutron stars with $\sim 2M_{\odot}$ (see e.g., [159]), and it has been explored by a number of authors in the last years [160–167]. However, no general consensus has been reached yet regarding the role played by the hyperonic three-body forces in solving the hyperon puzzle. A multi-Pomeron exchange potential (MPP) model to introduce a universal three-body repulsion among three baryons in the hyperonic matter EoS was proposed in [162,163,165]. This universal three-body repulsive potential was based on the extended soft core (ESC) baryon–baryon interaction of the Nijmegen group [48–50]. The strength of the MPP was determined by analyzing the nucleus–nucleus scattering with the use of a G-matrix folding potential derived from the ESC interaction complemented with the MPP and a three-nucleon attractive part, added phenomenologically in order to reproduce the nuclear saturation properties. The results of those works [162,163,165] showed that when the MPP contribution was taken into account, universally for all baryons, neutron star radii R at a typical mass $1.5M_{\odot}$ were predicted to be around 12.3–13.1 km [166], and a maximum mass of $\sim 2.2M_{\odot}$ was obtained. This result for the maximum mass is in contradiction with that reported in [161] where the case of a universal three-body repulsion was also analyzed. The authors of [161] used a model based on the BHF approach of hypernuclear matter using the Argonne V18 NN potential [182] and the Nijmegen YN soft core NSC89 one [44] supplemented with additional simple phenomenological density-dependent contact terms to establish numerically lower and upper limits to the effect of hyperonic three-body forces on the maximum mass of neutron stars. Assuming that the strength of these forces was either smaller than or as large as the pure nucleonic ones, the results reported in [161] showed that, although the employed hyperonic three-body forces stiffened the EoS, they were, however, unable to provide the repulsion needed to make the predicted maximum masses compatible with the recent observations. In [164], a Monte Carlo calculation of pure neutron matter with a non-vanishing Λ-hyperon concentration was carried out including NN, NNN, ΛN and NNΛ two- and three-body interactions. In particular, the NNΛ force used in this work was tuned in order to provide a reasonable description of the measured Λ separation energy of several hypernuclei [70]. The authors of this work concluded that, with the model they considered, the presence of hyperons in the core of neutron stars could not be satisfactorily established and, consequently, according to these authors, there is no clear incompatibility with astrophysical observations when the Λ is included. However, one should note, that the presence of protons, necessary to establish the correct β-equilibrium inside neutron stars and, thus, a proper treatment of nuclear matter was neglected in their calculation. Very recently, the authors [167] have studied the effects of chiral hyperonic three-body forces on neutron stars, showing that the inclusion of a moderate repulsive NNΛ force leads already to an EoS stiff enough such that the resulting neutron star maximum mass is compatible with the largest currently measured massed. These authors have also examined the effect of this NNΛ force on the separation energy of a Λ in some hypernuclei obtaining a good description of the experimental data. This is in agreement with the results of [183], where also a moderate hyperonic three-body force was found to be enough to reproduce

the binding energies of single-Λ hypernuclei, but contrary to the results reported in [70] where a very repulsive NNΛ was required to describe the data. In conclusion, it seems that although hyperonic three-body forces offer an interesting microscopic solution to the hyperon puzzle, the uncertainties associated to these forces are still too large to allow for a definite conclusion.

3.1.3. Quark Matter Phase Transition below the Hyperon Threshold

An early phase transition from hadronic matter to deconfined quark matter at densities below the hyperon threshold could provide the solution to the hyperon puzzle, as it has been suggested by several authors. In this case, massive stars could actually be hybrid stars with a stiff quark matter core. This solution, however, leads to a new question: can quarks provide the sufficient repulsion required to produce a $2M_{\odot}$ neutron star? In [168,169], the maximum mass was found to be in a relatively narrow interval, $\sim 1.4M_{\odot} < M_{max} <\sim 1.7M_{\odot}$ which is incompatible with the current observational limit of $2M_{\odot}$. To obtain values of M_{max} larger than $2M_{\odot}$, the interaction among quarks should fulfill two important and necessary conditions. First of all, it should be significantly repulsive, for example, in vector channels in order to guarantee that the EoS is stiff enough. Second, it should be strongly attractive in certain channels, leading to color superconductivity, so that the deconfined quark-matter phase is energetically favorable with respect to the hadronic one. Current theoretical descriptions of quark matter at high density rely on phenomenological models, which are constrained using the few available experimental information on high density baryonic matter from heavy-ion collisions. Several models of hybrid stars have been proposed in the recent years with the necessary properties to generate a $2M_{\odot}$ (see, e.g., [171–179]). Very recently, Shahrbaf et al. [178,179] have applied, for the first time, the finite-range polynomial interpolation method of Masuda et al. [184,185] for constructing a transition between hadronic and quark matter phases. The predicted maximum mass of the hybrid star is about $2.2M_{\odot}$ in agreement with current observations. The observation of $2M_{\odot}$ neutron stars, on the other hand, may also help constrain better the models of hybrid and strange stars (compact stars completely made of deconfined u, d and s quark matter), and improve our present understanding of the hadron–quark phase transition.

3.1.4. Δ Isobar and Kaon Condensation in Neutron Stars

An alternative possible solution to the hyperon puzzle that has been also considered is the appearance of other hadronic degrees of freedom, such as for instance the Δ isobar or meson condensates, that can push the onset of hyperons to higher densities. The presence of the Δ isobar in neutron stars was usually neglected because in former calculations its threshold density was found to be larger than the typical densities of neutron star cores. A few years ago, it has been shown [186], however, that the onset density of the Δ isobar depends crucially on the slope parameter L of the nuclear symmetry energy. Using recent experimental constraints and a state-of-the-art EoS, the authors of [186] have shown that the Δ isobar could actually appear at densities below the hyperon threshold. However, they found that, as soon as the Δ appears, the EoS becomes also considerably soft and, as a consequence, M_{max} is reduced to values below the current observational limits, giving rise to what they have named the "Δ puzzle". Very recently, using an RMF approach, the authors of [187] found, however, that the presence of the Δ isobar in the neutron star interior is compatible with the observation of $2\,M_{\odot}$ millisecond pulsars, provided that the couplings of the Δ to the σ and ω meson fields are at least 10% stronger than the corresponding ones of the nucleons. The possibility that pions or kaons form Bose–Einstein condensates in the interior of neutron stars has also been extensively considered in the literature [188–193]. However, as in the case of the hyperons or the Δ isobar, the appearance of a meson condensate induces also a strong softening of the EoS reducing the value of M_{max} below the current observational limits too.

3.2. Effect of Hyperons on Proto-Neutron Stars

Thermal effects and neutrino trapping affect the properties of newly born neutron stars during the first tens of seconds after their formation. In particular, the composition and the overall stiffness of the EoS of the star are strongly influenced by these two effects. Matter becomes more proton rich, the number of muons is significantly reduced and the onset of hyperons is shifted to higher densities [194–198]. Furthermore, the number of strange particles is on average smaller, and the EoS is stiffer in comparison with the cold and neutrino-free case.

A very important consequence of the neutrino trapping in dense matter is the possibility of having metastable neutron stars and a delayed formation of a "low mass" ($M = 1 - 2M_{\odot}$) black hole. To illustrate this, we show in Figure 6 the gravitational mass M_G of the star as a function of its baryonic mass M_B (proportional to the total number of baryons in the star) obtained by the authors of [197]. When hyperons are present in the star (Figure 6a), the deleptonization lowers the range of gravitational masses that can be supported by the EoS from about $1.59M_{\odot}$ to about $1.28M_{\odot}$ (see dotted horizontal lines in the figure). The neutron star baryonic mass can be considered constant during the evolution from the initial proto-neutron star configuration to the final neutrino-free one because most of the matter accretion on the forming neutron star happens in a very early stage after its birth (t < 1 s). For this particular calculation, proto-neutron stars born with gravitational masses between $1.28M_{\odot}$ and $1.59M_{\odot}$ (a baryonic mass between $1.40M_{\odot}$ and $1.72M_{\odot}$) will be stabilized by neutrino trapping effects long enough to carry out nucleosynthesis accompanying a Type-II supernova explosion. After neutrinos leave the star, the EoS is softened and it cannot support anymore the star against its own gravity and the newborn star collapses then to a black hole [194–196]. Conversely, when only nucleons are considered to be the relevant baryonic degrees of freedom (Figure 6b), no metastability occurs and a black hole is unlikely to be formed during the deleptonization because the gravitational mass increases during this stage which happens at (almost) constant baryonic mass. If a black hole were to form from a star with only nucleons, it is much more likely to form during the post-bounce accretion stage.

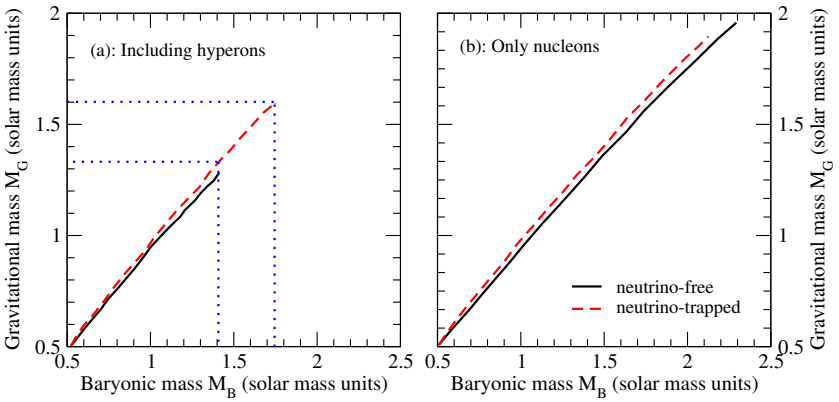

Figure 6. Gravitational mass as a function of the baryonic mass for neutrino-free (solid lines) and neutrino-trapped (dashed lines) matter. Panel (**a**) shows the results for matter containing nucleons and hyperons, whereas the results for pure nucleonic matter are shown in panel (**b**). Dotted horizontal and vertical lines show the window of metastability in the gravitational and baryonic masses. Figure adapted from [197].

3.3. Hyperons and Neutron Star Cooling

The cooling of a newly born hot neutron star is driven in a first stage by the neutrino emission from the interior, and later by the emission of photons at the surface. Depending on whether the number of involved baryons is one or two, neutrino emission reactions can

be classified as fast or slow processes, respectively. The simplest possible neutrino emission reaction is the well-known direct Urca process

$$n \to p + l + \bar{\nu}_l \,, \quad p + l \to n + \nu_l \,. \tag{14}$$

This is a fast mechanism which, due to momentum conservation, is only possible when the proton fraction exceeds a critical value $x_{DURCA} \sim 11\%$ to 15% [199]. Other neutrino reactions that lead to medium or slow cooling scenarios, but that are operative at any density and proton fraction, are the modified Urca processes:

$$N + n \to N + p + l + \bar{\nu}_l \,, \quad N + p + l \to N + n + \nu_l \,, \tag{15}$$

the bremsstrahlung:

$$N + N \to N + N + \nu + \bar{\nu} \,, \tag{16}$$

or the Cooper pair formation:

$$n + n \to [nn] + \nu + \bar{\nu} \,, \quad p + p \to [pp] + \nu + \bar{\nu}, \tag{17}$$

this last operating only when the temperature of the star drops below the critical temperature for neutron superfluidity or proton superconductivity.

The presence of hyperons can affect the cooling of neutron stars because they can modify neutrino emissivities allowing for additional cooling mechanisms such as, for example, the direct

$$Y \to B + l + \bar{\nu}_l \,, \quad B + l \to Y + \nu_l \,, \tag{18}$$

and modified

$$B' + Y \to B' + B + l + \bar{\nu}_l \,, \quad B' + B + l \to B' + Y + \nu_l \,, \tag{19}$$

hyperonic Urca processes. These additional neutrino emission reactions, however, can lead to temperatures at the surface of the star that are much lower than those observed, unless they are suppressed by hyperon pairing gaps. The study of hyperon superfluidity becomes then of particular interest because it could play a key role in the thermal history of neutron stars. Nevertheless, whereas the presence of superfluid neutrons in the inner crust of neutron stars, and that of superfluid neutrons together with superconducting protons in their quantum fluid interior are well established and have been the subject of many studies, a quantitative estimation of the hyperon pairing has not received so much attention, and just few calculations exist in the literature [200–206].

3.4. Hyperons and R-Modes

It is well known that if a neutron star rotates with a spin frequency above the so-called Kepler frequency Ω_K, i.e., the absolute maximum rotational frequency of a neutron star, then matter is ejected from the star's equator [207,208]. Different types of perturbations, however, can lead to instabilities that prevent the star from reaching rotational frequencies as high as Ω_K and set more stringent limits on their rotation [209]. One of these possible instabilities which is particularly interesting is the so-called r-mode instability [210,211]. It is a toroidal mode of oscillation whose restoring force is the Coriolis force which leads to the emission of gravitational waves in hot and rapidly rotating neutron stars through the Chandrasekhar–Friedman–Schutz mechanism [212–214]. The r-mode grows with the emission of gravitational waves whereas it is damped by dissipation mechanisms. The r-mode becomes unstable when the driving time of the gravitational radiation is shorter than the damping time associated to viscous processes. A rapidly rotating neutron star could transfer in this case a significant fraction of its angular momentum and rotational energy to the emitted gravitational waves.

Bulk (ξ) and shear (η) viscosities are the main dissipation mechanisms of r- and other pulsation modes. At high temperatures ($T > 10^9$ K), the bulk viscosity is the dominant mechanism and, therefore, it is the most important one for hot young neutron stars. It results from the variations in the pressure and the density induced by the oscillation mode which drives the star away from β-equilibrium. The weak interaction tries then to reestablish the equilibrium with the consequent dissipation of energy. If no hyperons or other exotic components are present in the neutron star interior, the bulk viscosity is mainly determined by the direct and modified Urca processes. However, as soon as hyperons appear, new mechanisms such as strong interaction reactions

$$Y + Y \leftrightarrow N + Y\,, \quad N + \Xi \leftrightarrow Y + Y\,, \quad Y + Y \leftrightarrow Y + Y\,, \tag{20}$$

weak non-leptonic hyperon reactions

$$N + N \leftrightarrow N + Y\,, \quad N + Y \leftrightarrow Y + Y\,, \tag{21}$$

or direct and modified hyperonic Urca (see Equations (18) and (19)) contribute to the bulk viscosity and dominate it for densities above 2–3 times the nuclear saturation density. Hyperon bulk viscosity has been considered by several authors, see, e.g., [215–229].

The time dependence of an r-mode oscillation is given by $e^{i\omega t - t/\tau(\Omega,T)}$ where ω is the frequency of the mode and

$$\frac{1}{\tau(\Omega,T)} = -\frac{1}{\tau_{GW}(\Omega)} + \frac{1}{\tau_{\xi}(\Omega,T)} + \frac{1}{\tau_{\eta}(\Omega,T)}\,, \tag{22}$$

is an overall timescale which describes both its exponential growth due to the gravitational wave emission and its decay due to the viscous damping, being τ_{GW}, τ_{ξ} and τ_{η} the time scales associated, respectively, to the gravitational wave emission and the bulk and shear viscosity dampings. If τ_{GW} is shorter than both τ_{ξ} and τ_{η}, the mode will exponentially grow, whereas in the opposite case, it will be quickly damped away. For each star at a given temperature T, one can define a critical angular velocity Ω_c as the smallest root of the equation

$$\frac{1}{\tau(\Omega_c,T)} = 0\,. \tag{23}$$

This equation defines the boundary of what is usually called the r-mode instability region. If the angular velocity of a neutron star is smaller than its corresponding Ω_c, then the star is stable against the r-mode instability. Conversely, a star with an angular velocity larger than Ω_c will develop an instability that will cause a rapid loss of angular momentum through gravitational radiation until its angular velocity falls below the critical value. As an example, on panel (a) of Figure 7, we show the r-mode instability region for a pure nucleonic (black solid line) and a hyperonic (red dashed line) star with $1.27 M_{\odot}$ both described using the BHF theory with realistic baryon interactions. On panel (b) of the figure, we show the contributions from direct and modified nucleonic Urca processes as well as from the weak non-leptonic process $n + n \leftrightarrow p + \Sigma^-$ included in the calculation of the bulk viscosity. As it is clearly seen, the r-mode instability is smaller for the hyperonic star. The reason is simply the increase of the bulk viscosity due to the presence of hyperons which makes the damping of the r-mode more efficient.

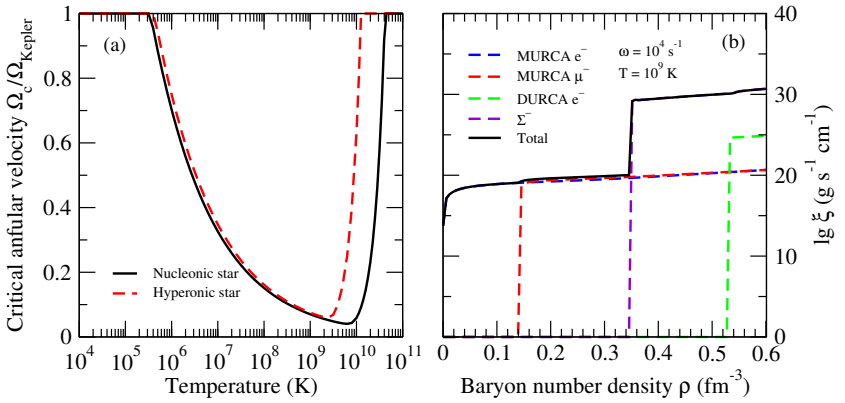

Figure 7. Panel (**a**): r-mode instability region for a pure nucleonic and a hyperonic star with $1.27 M_\odot$. The frequency of the mode is taken as $\omega = 10^4$ s^{-1}. Panel (**b**): Bulk viscosity as a function of the density for $T = 10^9$ K and $\omega = 10^4$ s^{-1}. Contributions from the direct and modified nucleonic Urca processes as well as from the weak non-leptonic process $n + n \leftrightarrow p + \Sigma^-$ are included.

4. Summary

In this work, we have briefly reviewed several topics related with the physics of hypernuclei and hyperons in neutron stars. In particular, we have revised the different production mechanisms of hypernclei as well as some aspects of their γ-ray spectroscopy and their weak decay modes. We have also given a few strokes on their theoretical description. We have discussed also the main effects of hyperons on the properties of neutron and proto-neutron stars with an emphasis on the well known "hyperon puzzle", the problem of the strong softening of the EoS of dense matter due to the appearance of hyperons which leads to maximum masses of compact stars that are not compatible with the recent observations of approximately $2 M_\odot$ millisecond pulsars. We have shortly reexamined some of the different solutions that have been proposed to tackle this problem. The first of the mechanisms we have revised consists of the inclusion of a repulsive hyperon–hyperon interaction through the exchange of vector mesons and it has been mainly explored in the context of RMF models. However, since presently there are not enough experimental data to constrain the YN and YY interaction accurately, it is not clear whether the large repulsion invoked in such models is realistic. The second one requires the inclusion of repulsive hyperonic three-body forces. However, at present, it is still an open issue whether these forces can, by themselves, solve completely the hyperon puzzle or not, although, it seems that even if they cannot provide the full answer they can contribute to it in an important way. The third possible solution to the problem we have reviewed is to consider the possibility of a phase transition to deconfined quark matter at densities below the hyperon threshold. However, the description of the quark phase via phenomenological models also suffers from uncertainties. Most models of hybrid stars unanimously agree that to construct massive neutron stars, it is required both a sufficiently stiff hadronic EoS as well as a color superconducting quark phase with strong interaction among quarks to provide sufficient repulsion. We have also briefly discussed a possible solution to the hyperon puzzle by invoking the appearance of other hadronic degrees of freedom such as the Δ isobar or meson condensates that push the onset of hyperons to higher densities. Finally, we have also revised how the presence of hyperons can affect the cooling of neutron stars and the r-mode instability window through modifications of the microscopic input of the weak interaction rates and transport coefficients, such as the bulk viscosity, of dense matter.

Funding: This research received no external funding.

Institutional Review Board Statement: Not applicable.

Informed Consent Statement: Not applicable.

Conflicts of Interest: The author declares no conflict of interest.

References

1. Lenske, H.; Dhar, M.; Gaitanos, T.; Cao, X. Baryons and baryon resonances in nuclear matter. *Prog. Part. Nucl. Phys.* **2018**, *98*, 119–206. [CrossRef]
2. Danysz, M.; Pniewski, J. Delayed disintegration of a heavy nuclear fragment: I. *Philos. Mag.* **1953**, *44*, 348–350. [CrossRef]
3. Hugenford, E.V. Experimental considerations in electromagnetic production of hypernuclei. *Prog. Theor. Phys. Suppl.* **1994**, *117*, 135–149.
4. Bianchin, S.; Achenbach, P.; Ajimura, S.; Borodina, O.; Fukuda, T.; Hoffmann, J.; Kavatsyuk, M.; Koch, K.; Koike, T.; Kurz, N.; et al.The HypHI project: Hypernuclear spectroscopy with stable heavy ion beams and rare isotope beams at GSI and Fair. *Int. J. Mod. Phys. E* **2009**, *18*, 2187–2191. [CrossRef]
5. Rappold, C.; Kim, E.; Nakajima, D.; Saito, T.R.; Bertini, O.; Bianchin, S.; Bozkurt, V.; Kavatsyuk, M.; Mab, Y.; Ma, F.; et al. Hypernuclear spectroscopy of products from ^{6}Li projectiles on a carbon target at 2AGeV. *Nucl. Phys. A* **2013**, *913*, 170–184. [CrossRef]
6. Shapiro, S.L.; Teukolsky, S.A. *Black Holes, White Dwarfs and Neutron Stars: The Physics of Compact Stars*; Wiley and Sons: Hoboken, NJ, USA, 1983.
7. Weber, F. *Pulsars as Astrophysical Laboratories for Nuclear and Particle Physics*; Institute of Physics Publishing: Bristol, UK, 1999.
8. Glendenning, N.K. *Compact Stars: Nuclear Physics, Particle Physics and General Relativity*, 2nd ed.; Springer: Berlin/Heidelberg, Germany, 2000.
9. Haensel, P.; Potekin, A.Y.; Yakovlev, D.G. *Neutron Stars 1: Equation of State*; Springer: Berlin/Heidelberg, Germany, 2007.
10. Rezzolla, L.; Pizzochero, P.; Jones, I.; Rea, N.; Vidaña, I. (Eds.) *The Physics and Astrophysics of Neutron Stars*; Springer Nature: Cham, Switzerland, 2018.
11. Balberg, S.; Gal, A. An effective equation of state for dense matter with strangeness. *Nucl. Phys. A* **1997** *625*, 435–472. [CrossRef]
12. Balberg, S.; Lichtenstadt, I.; Cook, G.B. Role of hyperons in neutron stars. *Astrophys. J. Suppl. Ser.* **1999**, *121*, 515. [CrossRef]
13. Millener, D.J.; Dover, C.B.; Gal, A. Λnucleus single-particle potentials. *Phys. Rev. C* **1988**, *38*, 2700. [CrossRef]
14. Yamamoto, Y.; Bandō, H.; Žofka, J. On the Λ-hypernuclear single particle energies. *Prog. Theor. Phys.* **1988**, *80*, 757–761. [CrossRef]
15. Fernández, F.; López–Arias, T.; Prieto, C. Skyrme-Hartree-Fock calculation of Λ-hypernuclear states from (π^+, K^+) reactions. *Z. Phys. A* **1989**, *334*, 349–354.
16. Lanskoy, D.E.; Yamamoto, Y. Skyrme-Hartree-Fock treatment of Λ and ΛΛ hypernuclei with G-matrix motivated interactions. *Phys. Rev. C* **1997**, *55*, 2330. [CrossRef]
17. Tretyakova, T.Y.; Lanskoy, D.E. Structure of neutron-rich Λ hypernuclei. *Eur. Phys. J. A* **1999**, *5*, 391–398. [CrossRef]
18. Cugnon, J.; Lejeune, A.; Schulze, H.-J. Hypernuclei in the Skyrme-Hartree-Fock formalism with a microscopic hyperon-nucleon force. *Phys. Rev. C* **2000**, *62*, 064308. [CrossRef]
19. Vidaña, I.; Polls, A.; Ramos, A.; Schulze, H.-J. Hypernuclear structure with the new Nijmegen potentials. *Phys. Rev. C* **2001** *64*, 044301. [CrossRef]
20. Zhou, X.-R.; Schulze, H.-J.; Sagawa, H.; Wu, C.-X.; Zhao, E.-G. Hypernuclei in the deformed Skyrme-Hartree-Fock approach. *Phys. Rev. C* **2007**, *76*, 034312. [CrossRef]
21. Zhou, X.-R.; Polls, A.; Schulze, H.-J.; Vidaña, I. Λ hyperons and the neutron drip line. *Phys. Rev. C* **2008**, *78*, 054306. [CrossRef]
22. Bednarek, I.; Haensel, P.; Zdunik, J.L.; Bejger, M.; Mańka, R. Hyperons in neutron-star cores and a $2M_{\odot}$ pulsar. *Astron. Astrophys.* **2012**, *543*, A157. [CrossRef]
23. Weissenborn, S.; Chatterjee, D.; Schaffner–Bielich, J. Hyperons and massive neutron stars: Vector repulsion and SU(3) symmetry. *Phys. Rev. C* **2012**, *85*, 065802. [CrossRef]
24. van Dalen, E.N.E.; Colucci, G.; Sedrakian, A. Constraining hypernuclear density functional with Λ-hypernuclei and compact stars. *Phys. Lett. B* **2014**, *734*, 383–387. [CrossRef]
25. Oertel, M.; Providência, C.; Gulminelli, F.; Raduta, A.R. Hyperons in neutron star matter within relativistic mean-field models. *J. Phys. G* **2015**, *42*, 075202. [CrossRef]
26. Maslov, K.A.; Kolomeitsev, E.E.; Voskresensky, D.N. Solution of the hyperon puzzle within a relativistic mean-field model. *Phys. Lett. B* **2015**, *748*, 369–375. [CrossRef]
27. Fortin, M.; Avancini, S.S.; Providência, C.; Vidaña, I. Hypernuclei and massive neutron stars. *Phys. Rev. C* **2017**, *95*, 065803. [CrossRef]
28. Pal, S.; Hanauske, M.; Zakout, I.; Stöcker, G.W. Neutron star properties in the quark-meson coupling model. *Phys. Rev. C* **1999**, *60*, 015802. [CrossRef]
29. Stone, J.R.; Guinchon, P.A.M.; Matevosyan, H.H.; Thomas, A.W. Cold uniform matter and neutron stars in the quark-meson-coupling model. *Nucl. Phys. A* **2007**, *792*, 341–369. [CrossRef]
30. Bombaci, I.; Panda, P.K.; Providência, C.; Vidaña, I. Metastability of hadronic compact stars. *Phys. Rev. D* **2008**, *77*, 083002. [CrossRef]
31. Carroll, J.D.; Leinweber, D.B.; Williams, A.G.; Thomas, A.W. Phase transition from quark-meson coupling hyperonic matter to deconfined quark matter. *Phys. Rev. C* **2009**, *79*, 045810. [CrossRef]
32. Miyatsu, T.; Saito, K. Effect of gluon and pion exchanges on hyperons in nuclear matter. *Prog. Theor. Phys.* **2009**, *122*, 1035–1044. [CrossRef]
33. Carroll, J.D. QMC and the nature of dense matter: Written in the stars? *AIP Conf. Proc.* **2010**, *1261*, 226–231.

34. Panda, P.K.; Santos, A.M.S.; Menezes, D.P.; Providência, C. Compact stars within a soft symmetry energy quark-meson-coupling model. *Phys. Rev. C* **2012**, *85*, 055802. [CrossRef]
35. Stone, J.R.; Dexheimer, V.; Guichon, P.A.M.; Thomas, A.W.; Typel, S. Equation of state of hot dense hyperonic matter in the Quark-Meson-Coupling (QMC-A) model. *Month. Not. R. Astron. Soc.* **2019**, *502*, 34767.
36. Antić, S.; Stone, J.R.; Thomas, A.W. Neutron stars from crust to core within the Quark-meson-coupling model. *EPJ Web Conf.* **2020**, *232*, 03001. [CrossRef]
37. Gaitanos, T.; Kaskulov, M. Momentum dependent mean-field dynamics of compressed nuclear matter and neutron stars. *Nucl. Phys. A* **2013**, *899*, 133–169. [CrossRef]
38. Moustakidis, C.C.; Gaitanos, T.; Margaritis, C.; Lalazissis, G.A. Bounds on the speed of sound in dense matter and neutron star structure. *Phys. Rev. C* **2017**, *95*, 045801. [CrossRef]
39. Gaitanos, T.; Chorozidou, A. Momentum dependent mean-fields of (anti)hyperons. *Nucl. Phys. A* **2021**, *1008*, 122153. [CrossRef]
40. Nagels, M.M.; Rijken, T.A.; de Swart, J.J. Determination of the mixing angle, F/(F +D) ratio, and coupling constants of the scalar-meson nonet. *Phys. Rev. Lett.* **1973**, *31*, 569. [CrossRef]
41. Nagels, M.M.; Rijken, T.A.; de Swart, J.J. Low-energy nucleon-nucleon potential from Regge-pole theory. *Phys. Rev. D* **1978**, *17*, 768. [CrossRef]
42. Machleidt, R.; Holinde, K.; Elster, C. The bonn meson-exchange model for the nucleon-nucleon interaction. *Phys. Rep.* **1987**, *149*, 1–89. [CrossRef]
43. Holzenkamp, B.; Holinde, K.; Speth, J. A meson exchange model for the hyperon-nucleon interaction. *Nucl. Phys. A* **1989**, *500*, 485–528. [CrossRef]
44. Maesen, P.M.M.; Rijken, T.A.; de Swart, J.J. Soft-core baryon-baryon one-boson-exchange models. II. Hyperon-nucleon potential. *Phys. Rev. C* **1989**, *40*, 2226. [CrossRef]
45. Rijken, T.A.; Stoks, V.G.J.; Yamamoto, Y. Soft-core hyperon-nucleon potentials. *Phys. Rev. C* **1999**, *59*, 21. [CrossRef]
46. Stoks, V.G.J.; Rijken, T.A. Soft-core baryon-baryon potentials for the complete baryon octet. *Phys. Rev. C* **1999**, *59*, 3009. [CrossRef]
47. Haidenbauer, J.; Meissner, U.-G. Jülich hyperon-nucleon model revisited. *Phys. Rev. C* **2005**, *72*, 044005. [CrossRef]
48. Rijken, T.A. Extended-soft-core baryon-baryon model. I. Nucleon-nucleon scattering with the ESC04 interaction. *Phys. Rev. C* **2006**, *73*, 044007. [CrossRef]
49. Rijken, T.A.; Yamamoto, Y. Extended-soft-core baryon-baryon model. II. Hyperon-nucleon interaction. *Phys. Rev. C* **2006**, *73*, 044008. [CrossRef]
50. Rijken, T.A.; Nagels, M.M.; Yamamoto, Y. Baryon-baryon interactions. *Prog. Theor. Phys. Suppl.* **2010**, *185*, 14. [CrossRef]
51. Weinberg, S. Nuclear forces from chiral lagrangians. *Phys. Lett. B* **1991**, *251*, 288. [CrossRef]
52. Weinberg, S. Effective chiral lagrangians for nucleon-pion interactions and nuclear forces. *Nucl. Phys. B* **1991**, *363*, 3–18. [CrossRef]
53. Entem, D.R.; Machleidt, R. Accurate charge-dependent nucleon-nucleon potential at fourth order of chiral perturbation theory. *Phys. Rev. C* **2003**, *68*, 041001. [CrossRef]
54. Epelbaum, E.; Glöcke, W.; Meissner, U.-G. The two-nucleon system at next-to-next-to-next-to-leading order. *Nucl. Phys. A* **2005**, *747*, 362–424. [CrossRef]
55. Entem, D.R.; Machleidt, R.; Nosyk, Y. High-quality two-nucleon potentials up to fifth order of the chiral expansion. *Phys. Rev. C* **2017**, *96*, 024004. [CrossRef]
56. Epelbaum, E. Few-nucleon forces and systems in chiral effective field theory. *Prog. Nucl. Part. Phys.* **2006**, *57*, 654–741. [CrossRef]
57. Polinder, H.; Haidenbauer, J.; Meissner, U.-G. Hyperon–nucleon interactions—A chiral effective field theory approach. *Nucl. Phys. A* **2006**, *779*, 244–266. [CrossRef]
58. Haidenbauer, J.; Petschauer, S.; Kaiser, N.; Meissner, U.-G.; Nogga, A.; Weise, W. Hyperon–nucleon interaction at next-to-leading order in chiral effective field theory. *Nucl. Phys. A* **2013**, *915*, 24–58. [CrossRef]
59. Haidenbauer, J.; Meissner, U.-G.; Nogga, A. Hyperon-nucleon interaction within chiral effective field theory revisited. *Eur. Phys. J. A* **2020**, *56*, 91. [CrossRef]
60. Schulze, H.-J.; Baldo, M.; Lombardo, U.; Cugnon, J.; Lejeune, A. Hypernuclear matter in the Brueckner-Hartree-Fock approximation. *Phys. Lett. B* **1995**, *355*, 21–26. [CrossRef]
61. Schulze, H.-J.; Baldo, M.; Lombardo, U.; Cugnon, J.; Lejeune, A. Hyperonic nuclear matter in Brueckner theory. *Phys. Rev. C* **1998**, *57*, 704. [CrossRef]
62. Baldo, M.; Burgio, G.F.; Schulze, H.-J. Onset of hyperon formation in neutron star matter from Brueckner theory. *Phys. Rev. C* **1998**, *58*, 3688. [CrossRef]
63. Baldo, M.; Burgio, G.F.; Schulze, H.-J. Hyperon stars in the Brueckner-Bethe-Goldstone theory. *Phys. Rev. C* **2000**, *61*, 055801. [CrossRef]
64. Vidaña, I.; Polls, A.; Ramos, A.; Hjorth-Jensen, M.; Stoks, V.G.J. Strange nuclear matter within Brueckner-Hartree-Fock theory. *Phys. Rev. C* **2000**, *61*, 025802. [CrossRef]
65. Vidaña, I.; Polls, A.; Ramos, A.; Engvik, L.; Hjorth-Jensen, M. Hyperon-hyperon interactions and properties of neutron star matter. *Phys. Rev. C* **2000**, *62*, 035801. [CrossRef]
66. Schulze, H.-J.; Polls, A.; Ramos, A.; Vidaña, I. Maximum mass of neutron stars. *Phys. Rev. C* **2006**, *73*, 058801. [CrossRef]
67. Schulze, H.-J.; Rijken, T. Maximum mass of hyperon stars with the Nijmegen ESC08 model. *Phys. Rev. C* **2011**, *84*, 035801. [CrossRef]

68. Dapo, H.; Schaefer, B.-J.; Wambach, J. Appearance of hyperons in neutron stars. *Phys. Rev. C* **2010**, *81*, 035803. [CrossRef]
69. Sammarruca, F. Effect of Λ hyperons on the nuclear equation of state in a Dirac- Brueckner-Hartree-Fock model. *Phys. Rev. C* **2009**, *79*, 034301. [CrossRef]
70. Lonardoni, D.; Pederiva, F.; Gandolfi, S. Accurate determination of the interaction between Λ hyperons and nucleons from auxiliary field diffusion Monte Carlo calculations. *Phys. Rev. C* **2014**, *89*, 014314. [CrossRef]
71. Petschauer, S.; Haidenbauer, J.; Kaiser, N.; Meissner, U.-G.; Weise, W. Hyperons in nuclear matter from SU(3) chiral effective field theory. *Eur. Phys. J. A* **2016**, *52*, 15. [CrossRef]
72. Haidenbauer, J.; Meissner, U.-G.; Kaiser, N.; Weise, W. Lambda-nuclear interactions and hyperon puzzle in neutron stars. *Eur. Phys. J. A* **2017**, *53*, 121. [CrossRef]
73. Kohno, M. Comparative study of hyperon-nucleon interactions in a quark model and in chiral effective field theory by low-momentum equivalent interactions and G matrices. *Phys. Rev. C* **2010**, *81*, 014003. [CrossRef]
74. Kohno, M. Single-particle potential of the Λ hyperon in nuclear matter with chiral effective field theory NLO interactions including effects of YNN three-baryon interactions. *Phys. Rev. C* **2018**, *97*, 035206. [CrossRef]
75. Ohnishi, A.; Morita, K.; Miyahara, K.; Hyodo, T. Hadron–hadron correlation and interaction from heavy–ion collisions. *Nucl. Phys. A* **2016**, *954*, 294–307. [CrossRef]
76. Adamczewski–Musch, J.; Agakishiev, G.; Arnold, O.; Atomssa, E.T.; Behnke, C.; Berger-Chen, J.C.; Hades Collaboration. Λp interaction studied via femtoscopy in $p \rightarrow Nb$ reactions at $\sqrt{s_{NN}} = 3.18$ GeV. *Phys. Rev. C* **2016**, *94*, 025201. [CrossRef]
77. Hatsuda, T.; Morita, K.; Ohnishi, A.; Sasaki, K. pΞ$^-$ correlation in relativistic heavy ion collisions with nucleon-hyperon Interaction from Lattice QCD. *Nucl. Phys. A* **2017**, *967*, 856–859. [CrossRef]
78. Mihaylov, D.L.; Sarti, V.M.; Arnold, O.W.; Fabbietti, L.; Holweger, B.; Mathis, A.M. A femtoscopic correlation analysis tool using the Schrödinger equation (CATS). *Eur. Phys. J. C* **2018**, *78*, 394. [CrossRef]
79. Acharya, S.; Adamová, D.; Adhya, S.P.; Adler, A.; Adolfsson, J.; Aggarwal, M.M.; A Large Ion Collider Experiment Collaboration. First observation of an attractive interaction between a proton and a cascade baryon. *Phys. Rev. Lett.* **2019**, *123*, 112002. [CrossRef] [PubMed]
80. Acharya, S.; Adamová, D.; Adolfsson, J.; Aggarwal, M.M.; Rinella, G.A.; Agnello, M.; ALICE Collaboration. p-p, p-Λ, and Λ-Λ correlations studied via femtoscopy in pp reactions at $s = 7$ TeV. *Phys. Rev. C* **2019**, *99*, 024001. [CrossRef]
81. Acharya, S.; Adamová, D.; Adhya, S.P.; Adler, A.; Adolfsson, J.; Aggarwal, M.M.; Castro, A.J.; ALICE Collaboration. Study of the Λ-Λ interaction with femtoscopy correlations in pp and p-Pb collisions at the LHC. *Phys. Lett. B* **2019**, *797*, 134822. [CrossRef]
82. Acharya, S.; Adamová, D.; Adler, A.; Adolfsson, J.; Aggarwal, M.M.; Rinella, G.A.; Casula, E.A.R.; ALICE Collaboration. Investigation of the p-Σ^0 interaction via femtoscopy in pp collisions. *Phys. Lett. B* **2020**, *805*, 135419. [CrossRef]
83. Fabbietti, L.; Sarti, V.M.; Vázquez Doce, O.V. Hadron-hadron interactions measured by ALICE at the LHC. *arXiv* **2012**, arXiv.2012.09806.
84. Tolós, L.; Fabbietti, L. Strangeness in nuclei and neutron stars. *Prog. Part. Nucl. Phys.* **2020**, *112*, 103770. [CrossRef]
85. ALICE Collaboration. Unveiling the strong interaction among hadrons at the LHC. *Nature* **2020**, *588*, 232–238. [CrossRef]
86. Pratt, S. Pion interferometry of quark-gluon plasma. *Phys. Rev. D* **1986**, *33*, 1314. [CrossRef]
87. Lisa, M.A.; Pratt, S.; Soltz, R.; Wiedemman, U. Femtoscopy in relativistic heavy ion collisions: Two decades of progress. *Ann. Rev. Nucl. Part. Sci.* **2005**, *55*, 357–402. [CrossRef]
88. Beane, S.R.; Savage, M. Nucleon–nucleon interactions on the lattice. *Phys Lett. B* **2002**, *535*, 177–180. [CrossRef]
89. Ishii, N.; Aoki, S.; Hatsuda, T. Nuclear force from lattice QCD. *Phys. Rev. Lett.* **2007**, *99*, 022001. [CrossRef] [PubMed]
90. Aoki, S.; Hatsuda, T.; Ishii, N. Theoretical foundation of the nuclear force in QCD and its applications to central and tensor forces in quenched lattice QCD simulations. *Prog. Theor. Phys.* **2010**, *123*, 89–128. [CrossRef]
91. Beane, S.; Detmold, W.; Orginos, K.; Savage, M. Nuclear physics from lattice QCD. *Prog. Part. Nucl. Phys.* **2011**, *66*, 1–40. [CrossRef]
92. Aoki, S. Hadron interactions in lattice QCD. *Prog. Part. Nucl. Phys.* **2011**, *66*, 687–726. [CrossRef]
93. Aoki, S.; Doi, T.; Hatsuda, T.; Ikeda, Y.; Inoue, T.; Ishii, N.; Murano, K.; Nemura, H.; Sasaki, K. Lattice quantum chromodynamical approach to nuclear physics. *Prog. Theor. Exp. Phys.* **2012**, *1*, 01A105. [CrossRef]
94. Nemura, H.; Aoki, S.; Gongyo, S.; Hatsuda, T.; Ikeda, Y.; Inoue, T.; Iritani, T.; Ishii, N.; Miyamoto, T.; Sasaki, K.; et al. Lambda-Nucleon and Sigma-Nucleon interactions from lattice QCD with physical masses. *arXiv* **2017**, arXiv:1702.00734.
95. Doi, T.; Aoki, S.; Doi, T.; Gongyo, S.; Hatsuda, T.; Ikeda, Y.; Inoue, T.; Iritani, T.; Ishii, N.; Miyamoto, T.; et al. Baryon interactions from lattice QCD with physical masses—overview and S=0, −4 sectors—. *arXiv* **2017**, arXiv:1702.01600.
96. HALQCD Collaboration. Baryon interactions from lattice QCD with physical masses—S = −3 sector: ΞΣ and ΞΛ − ΞΣ—. *PoS* **2017**, *256*, 127.
97. HALQCD Collaboration. Baryon interactions from lattice QCD with physical masses—S = −2 sector—. *arXiv* **2017**, arXiv:1702.06241.
98. Doi, T.; Aoki, S.; Doi, T.; Gongyo, S.; Hatsuda, T.; Ikeda, Y.; Inoue, T.; Iritani, T.; Ishii, N.; Miyamoto, T.; et al. Baryon interactions from lattice QCD with physical quark masses—Nuclear forces and ΞΞ forces—. *EPJ Web. Conf.* **2018**, *175*, 05009. [CrossRef]
99. Nemura, H.; Aoki, S.; Gongyo, S.; Hatsuda, T.; Ikeda, Y.; Inoue, T.; Iritani, T.; Ishii, N.; Miyamoto, T.; Sasaki, K.; et al. Baryon interactions from lattice QCD with physical masses—strangeness S = −1 sector—. *EPJ Web. Conf.* **2018**, *175*, 05030. [CrossRef]

100. Iritani, T.; Aoki, S.; Doi, T.; Etminan, F.; Gongyo, S.; Hatsuda, T.; Ikeda, Y.; Inoue, T.; Ishii, N.; Miyamoto, T.; et al. NΩ dibaryon from lattice QCD near the physical point. *Phys. Lett. B* **2019**, *792*, 284–289. [CrossRef]
101. Iritani, T.; Aoki, S.; Doi, T.; Gongyo, S.; Hatsuda, T.; Ikeda, Y.; Inoue, T.; Ishii, N.; Nemura, H.; Sasaki, K. Systematics of the HAL QCD potential at low energies in lattice QCD. *Phys. Rev. D* **2019**, *99*, 014514. [CrossRef]
102. Sasaki, K.; Aoki, S.; Doi, T.; Gongyo, S.; Hatsuda, T.; Ikeda, Y.; Inoue, T.; Iritani, T.; Ishiie, N.; Murano, K.; et al. ΛΛ and $N\Sigma$ interactions from lattice QCD near the physical point. *Nucl. Phys. A* **2020**, *998*, 121737. [CrossRef]
103. Beane, S.R.; Chang, E.; Cohen, S.D.; Detmold, W.; Lin, H.W.; Luu, T.C.; Orginos, K.; Parreño, A.; Savage, M.J.; Walker-Loud, A. Hyperon-nucleon interactions from Quantum Chromodynamics and the composition of dense nuclear matter. *Phys. Rev. Lett.* **2012**, *109*, 172001. [CrossRef] [PubMed]
104. Orginos, K.; Parreno, A.; Savage, M.J.; Beane, S.R.; Chang, E.; Detmold, W. Two nucleon systems at $m_\pi \sim 450$ MeV from lattice QCD. *Phys. Rev. D* **2015**, *92*, 114512. [CrossRef]
105. Illa, M.; Beane, S.R.; Chang, E.; Davoudi, Z.; Detmold, W.; Murphy, D.J.; Orginos, K.; Parreño, A.; Savage, M.J.; Shanahan, P.E.; et al. Low-energy scattering and effective interactions of two baryons at $m_\pi \sim 450$ MeV from lattice quantum chromodynamics. *Phys. Rev. D* **2021**, *103*, 054508. [CrossRef]
106. Botta, E.; Bressani, T.; Garbarino, G. Strangeness nuclear physics: A critical review on selected topics. *Eur. Phys. J. A* **2012**, *48*, 41–64. [CrossRef]
107. Gal, A.; Hugerford, E.V.; Millener, D.J. Strangeness in nuclear physics. *Rev. Mod. Phys.* **2016**, *88*, 035004. [CrossRef]
108. Hugenford, E.V. Topics in strangeness nuclear physics. *Lect. Notes Phys.* **2007**, *274*, 1.
109. Takahashi, H.; Ahn, J.K.; Akikawa, H.; Aoki, S.; Arai, K.; Bahk, S.Y.; Observation of a ${}^{6}_{\Lambda\Lambda}$He double hypernucleus. *Phys. Rev. Lett.* **2001**, *87*, 212502. [CrossRef] [PubMed]
110. Khaustov, P. Evidence of Ξ hypernuclear production in the ^{12}C$(K^-, K^+)^{12}_{\Xi^-}$Be reaction. *Phys. Rev. C* **2000**, *61*, 054603. [CrossRef]
111. Friedman, E.; Gal, A. Constraints on Ξ^- nuclear interactions from capture events in emulsion. *Phys. Lett. B* **2021**, *820*, 136555. [CrossRef]
112. Nakazawa, K.; Endo, Y.; Fukunaga, S.; Hoshino, K.; Hwang, S.H.; Imai, K.; Ito, H.; Itonaga, K.; Kanda, T.; Kawasaki, M.; et al. The first evidence of a deeply bound state of Ξ^--^{14}N system. *Prog. Theor. Exp. Phys.* **2015**, *2015*, 033D02. [CrossRef]
113. Hiyima, E.; Nakazawa, K. Structure of S=-2 Hypernuclei and Hyperon–Hyperon Interactions. *Ann. Rev. Nucl. Part. Sci.* **2018**, *68*, 131–159. [CrossRef]
114. Hayakawa, S.H.; Agari, K.; Ahn, J.K.; Akaishi, T.; Akazawa, Y.; Ashikaga, S.; J-PARC E07 Collaboration. Observation of Coulomb-assisted nuclear bound state of $\Xi^- - {}^{14}N$ system. *Phys. Rev. Lett.* **2021**, *126*, 062501. [CrossRef]
115. Hashimoto, O.; Tamura, H. Spectroscopy of Λ hypernuclei *Prog. Part. Nucl. Phys.* **2006**, *57*, 564. [CrossRef]
116. Ukai, M. γ-ray spectroscopy of ${}^{16}_{\Lambda}$O and ${}^{15}_{\Lambda}$N hypernuclei via the ^{16}O$(K^-, \pi^-\gamma)$ reaction. *Phys. Rev. C* **2008**, *77*, 054315. [CrossRef]
117. Bauer, E.; Garbarino, G.; Parreño, A.; Ramos, A. Microscopic approach to the proton asymmetry in the nonmesonic weak decay of Λ hypernuclei. *Phys. Rev. C* **2012**, *85*, 024321. [CrossRef]
118. Bauer, E.; Garbarino, G.; Rodríguez Peña, C.A. Nonmesonic weak decay of Λ hypernuclei: The ΛN-ΣN coupling. *Phys. Rev. C* **2017**, *96*, 044303. [CrossRef]
119. Parreño, A.; Bennhold, C.; Holstein, B.R. $\Lambda N \to NN$ weak interaction in effective-field theory. *Phys. Rev. C* **2004**, *70*, 051601(R). [CrossRef]
120. Pérez-Obiol, A.; Entem, D.R.; Juliá-Díaz, B.; Parreño, A. One-loop contributions in the effective field theory for the $\Lambda N \to NN$ transition. *Phys. Rev. C* **2013**, *87*, 044614. [CrossRef]
121. Alberico, W.M.; Garbarino, G. Weak decay of Λ hypernuclei. *Phys. Rep.* **2002**, *369*, 1. [CrossRef]
122. Parreño, A. Weak decays of hypernuclei. *Lect. Note Phys.* **2007**, *724*, 141–189.
123. Alberico, W.M.; De Pace, A.; Garbarino, G.; Ramos, A. Weak decays of medium and heavy Λ hypernuclei. *Phys. Rev. C* **2000**, *61*, 044314. [CrossRef]
124. Bouyssy, A.; Hüfner, J. Hypernuclei with $A \geq 12$. *Phys. Lett. B* **1976**, *27*, 276. [CrossRef]
125. Bouyssy, A. Strangeness exchange reactions and hypernuclear spectroscopy. *Phys. Lett. B* **1979**, *84*, 41–45. [CrossRef]
126. Dover, C.D.; Liedking, L.; Walker, G.E. Hypernuclear physics with pions. *Phys. Recv. C* **1980**, *22*, 2073. [CrossRef]
127. Motoba, T.; Bandō, H.; Wünsch, R.; Žofka, J. Hypernuclear production by the (π^+, K^+) reaction. *Phys. Rev. C* **1988**, *32*, 1322. [CrossRef] [PubMed]
128. Boguta, J.; Bohrmann, S. Relativistic quantum field theory of a hypernuclei. *Phys. Lett. B* **1981**, *102*, 93–96. [CrossRef]
129. Mareš, J.; Žofka, J. On Λ-hyperon(s) in the nuclear medium. *Z. Phys. A* **1989**, *333*, 209.
130. Glendenning, N.K.; Von-Eiff, D.; Haft, M.; Lenske, H.; Weigel, M.K. Relativistic mean-field calculations of Λ and Σ hypernuclei. *Phys. Rev. C* **1993**, *48*, 889. [CrossRef] [PubMed]
131. Mareš, J.; Jennings, B.K. Relativistic description of Λ, Σ , and Ξ hypernuclei. *Phys. Rev. C* **1993**, *49*, 2472. [CrossRef]
132. Sugahara, Y.; Toki, H. Relativistic mean field theory for lambda hypernuclei and neutron stars. *Prog. Theor. Phys.* **1994**, *92*, 803–813. [CrossRef]
133. Lombard, R.J.; Marcos, S.; Mareš, J. Description of hypernuclei in the scalar derivative coupling model. *Phys. Rev. C* **1995** *51*, 1784. [CrossRef]
134. Ma, Z.; Speth, J.; Krewald, S.; Chen, B.; Reuber, A. Hypernuclei with meson-exchange hyperon-nucleon interactions. *Nucl. Phys. A* **1996**, *608*, 305–315. [CrossRef]

135. Ineichenm, F.; Von-Eiff, D.; Weigel, M.K. A density-dependent relativistic Hartree approach for hypernuclei. *J. Phys. G* **1996** *22*, 1421. [CrossRef]
136. Tsushima, K.; Saito, K.; Thomas, A.W. Self-consistent description of Λ hypernuclei in the quark-meson coupling model. *Phys. Lett. B* **1997**, *411*, 9–18. [CrossRef]
137. Tsushima, K.; Saito, K.; Haidenbauer, J.; Thomas, A.W. The quark-meson coupling model for Λ, Σ and Ξ hypernuclei. *Nucl. Phys. A* **1998**, *630*, 691–718. [CrossRef]
138. Brockmann, R.; Weise, W. Relativistic single particle motion and spin-orbit coupling in nuclei and hypernuclei. *Nucl. Phys. A* **1981**, *355*, 365–382. [CrossRef]
139. Chiapparini, M.; Gattone, A.O.; Jennings, B.K. Dirac phenomonology and the Λ-nucleus potential. *Nucl. Phys. A* **1991**, *529*, 589–597. [CrossRef]
140. Yamamoto, Y.; Bandō, H. Chapter II. baryon-baryon interactions and single-particle aspects of hypernuclei. *Prog. Theor. Phys. Suppl.* **1985**, *81*, 9–41. [CrossRef]
141. Yamamoto, Y.; Bandō, H. Hypernuclear properties derived from the Nijmegen soft-core OBE potential. *Prog. Theor. Phys.* **1990**, *83*, 254–264. [CrossRef]
142. Yamamoto, Y.; Reuber, A.; Himeno, H.; Nagata, S.; Motoba, T. Hypernuclear properties derived from the Jülich hyperon-nucleon interaction (in comparison with the Nijmegen interactions). *Czec. J. Phys.* **1992**, *42*, 1249–1260. [CrossRef]
143. Yamamoto, Y.; Motoba, T.; Himeno, H.; Ikeda, K.; Nagata, S. Hyperon-nucleon and hyperon-hyperon interactions in nuclei. *Prog. Theor. Phys. Suppl.* **1994**, *117*, 361–389. [CrossRef]
144. Halderson, D. G-matrix calculations in finite hypernuclei. *Phys. Rev. C* **1993**, *48*, 581. [CrossRef]
145. Hjorth–Jensen, M.; Polls, A.; Ramos, A.; Müther, H. Self-energy of Λ in finite nuclei. *Nucl. Phys. A* **1996**, *605*, 458. [CrossRef]
146. Vidaña, I.; Polls, A.; Ramos, A.; Hjorth–Jensen, M. Hyperon properties in finite nuclei using realistic YN interactions. *Nucl. Phys. A* **1998**, *644*, 201–220. [CrossRef]
147. Haidenbauer, J.; Vidaña, I. Structure of single-Λ hypernuclei with chiral hyperon-nucleon potentials. *Eur. Phys. J. A* **2020**, *56*, 55. [CrossRef]
148. Lonardoni, D.; Gandolfi, S.; Pederiva, F. Effects of the two-body and three-body hyperon-nucleon interactions in Λ hypernuclei. *Phys. Rev. C* **2013**, *87*, 041303(R). [CrossRef]
149. Beane, S.R.; Chang, E.; Cohen, S.D.; Detmold, W.; Lin, H.W.; Luu, T.C.; Orginos, K.; Parreño, A.; Savage, M.J.; Walker-Loud, A. Light nuclei and hypernuclei from quantum chromodynamics in the limit of SU(3) flavor symmetry. *Phys. Rev. D* **2013**, *87*, 034506. [CrossRef]
150. Robertson, N.J.; Dickhoff, W.H. Correlation effects on Λ propagation in nuclear matter. *Phys. Rev. C* **2004**, *70*, 044301. [CrossRef]
151. Vidaña, I. Single-particle spectral function of the Λ hyperon in finite nuclei. *Nucl. Phys. A* **2017**, *958*, 48–70. [CrossRef]
152. Botta, E.; Bressani, T.; Felicello, A. On the binding energy and the charge symmetry breaking in $A \leq 16$ Λ-hypernuclei. *Nucl. Phys. A* **2017**, *960*, 165–179. [CrossRef]
153. Pile, P.H.; Bart, S.; Chrien, R.E.; Millener, D.J.; Sutter, R.J.; Tsoupas, N.; Peng, J.-C.; Mishra, C.S.; Hungerford, E.V.; Reidy, J.; et al. Study of hypernuclei by associated production. *Phys. Rev. Lett.* **1991**, *66*, 2585. [CrossRef]
154. Ambartsumyan, V.A.; Saakyan, G.S. The degenerate superdense gas of elementary particles. *Sov. Astron.* **1960**, *4*, 187.
155. Champion, D.J.; Ransom, S.M.; Lazarus, P.; Camilo, F.; Bassa, C.; Kaspi, V.M.; Nice, D.J.; Freire, P.C.C.; Stairs, I.H.; van Leeuwen, J.; et al. An eccentric binary pulsar in the galatic plane. *Science* **2008**, *320*, 1309–1312. [CrossRef] [PubMed]
156. Demorest, P.; Pennucci, T.; Ransom, S.M.; Roberts, M.S.E.; Hessels, J.W.T. A two-solar-mass neutron star measured using Shapiro delay. *Nature* **2010**, *467*, 1081–1083. [CrossRef]
157. Antoniadis, J.; Freire, P.C.; Wex, N.; Tauris, T.M.; Lynch, R.S.; Van Kerkwijk, M.H.; Kramer, M.; Bassa, C.; Dhillon, V.S. A massive pulsar in a compact relativistic binary. *Science* **2013**, *340*, 1233232. [CrossRef]
158. Cromartie, H.T.; Fonseca, E.; Ransom, S.M.; Demorest, P.B.; Arzoumanian, Z.; Blumer, H.; Brook, P.R.; DeCesar, E.M.; Dolch, T.; Ellis, J.A.; et al. Relativistic Shapiro delay measurements of an extremely massive millisecond pulsar. *Nat. Astron.* **2019**, *4*, 72–76. [CrossRef]
159. Takatsuka, T.; Nishizaki, S.; Yamamoto, Y. Necessity of extra repulsion in hypernuclear systems: Suggestion from neutron stars. *Eur. Phys. J. A* **2002**, *13*, 213–215. [CrossRef]
160. Takatsuka, T.; Nishizaki, S.; Tamagaki, R. Three-body force as an extra repulsion suggested from hyperon- mixed neutron stars. *Prog. Theor. Phys. Suppl.* **2008**, *174*, 80–83. [CrossRef]
161. Vidaña, I.; Logoteta, D.; Providência, C.; Polls, A.; Bombaci, I. Estimation of the effect of hyperonic three-body forces on the maximum mass of neutron stars. *Eur. Phys. Lett.* **2011**, *94*, 11002. [CrossRef]
162. Yamamoto, Y.; Furumotom, T.; Yasutake, B.; Rijken, T.A. Multi-Pomeron repulsion and the neutron-star mass. *Phys. Rev. C* **2013**, *88*, 022801. [CrossRef]
163. Yamamoto, Y.; Furumoto, T.; Yasutake, B.; Rijken, T.A. Hyperon mixing and universal many-body repulsion in neutron stars. *Phys. Rev. C* **2014**, *90*, 045805. [CrossRef]
164. Lonardoni, D.; Lovato, A.; Gandolfi, S.; Pederiva, F. Hyperon puzzle: Hints from quantum Monte Carlo calculations. *Phys. Rev. Lett.* **2014**, *114*, 092301. [CrossRef] [PubMed]
165. Yamamoto, Y.; Furumoto, T.; Yasutake, N.; Rijken, T.A. Hyperon-mixed neutron star with universal many-body repulsion. *Eur. Phys. J. A* **2016**, *52*, 19. [CrossRef]

166. Yamamoto, Y.; Togashi, H.; Tamagawa, T.; Furumoto, T.; Yasutake, N.; Rijken, T.A. Neutron-star radii based on realistic nuclear interactions. *Phys. Rev. C* **2017**, *96*, 065804. [CrossRef]
167. Logoteta, D.; Vidaña, I.; Bombaci, I. Impact of chiral hyperonic three-body forces on neutron stars. *Eur. Phys. J. A* **2019**, *55*, 207. [CrossRef]
168. Burgio, G.F.; Baldo, M.; Sahu, P.K.; Schulze, H.-J. Hadron-quark phase transition in dense matter and neutron stars. *Phys. Rev. C* **2002**, *66*, 025802. [CrossRef]
169. Burgio, G.F.; Baldo, M.; Sahu, P.K.; Santra, A.B.; Schulze, H.-J. Maximum mass of neutron stars with a quark core. *Phys. Lett. B* **2002**, *526*, 19–26. [CrossRef]
170. Alford, M.; Blaschke, D.; Drago, A.; Klähn, T.; Pagliara, G.; Schaffner–Bielich, J. Quark matter in compact stars? *Nature* **2007**, *445*, E7. [CrossRef] [PubMed]
171. Özel, F.; Psaltis, D.; Ransom, S.; Demorest, P.; Alford, M. The massive pulsar PSR J1614–2230: Linking quantum chromodynamics, gamma-ray bursts, and gravitational wave astronomy. *Astrophys. J. Lett.* **2010**, *724*, L199. [CrossRef]
172. Weissenborn, S.; Sagert, I.; Pagliara, G.; Hempel, M.; Schaeffner–Bielich, J. Quark matter in massive compact stars. *Astophys. J. Lett.* **2011**, *740*, L14. [CrossRef]
173. Schramm, S.; Negreiros, R.; Stenheimer, J.; Schürhoff, T.; Dexheimer, V. Properties and stability of hybrid stars. *Act. Phys. Pol. B* **2012**, *43*, 749. [CrossRef]
174. Bonanno, L.; Sedrakian, A. Composition and stability of hybrid stars with hyperons and quark color-superconductivity. *Astron. Astrophys.* **2012**, *539*, A16. [CrossRef]
175. Łastowiecki, R.; Blaschke, D.; Grigorian, H.; Typel, S. Strangeness in the cores of neutron stars. *Acta Phys. Polon. Suppl.* **2012**, *5*, 535. [CrossRef]
176. Zdunik, J.L.; Haensel, P. Maximum mass of neutron stars and strange neutron-star cores. *Astron. Astrophys.* **2013**, *551*, A61. [CrossRef]
177. Klähn, T.; Blaschke, D.; Łastowiecki, D. Implications of the measurement of pulsars with two solar masses for quark matter in compact stars and heavy-ion collisions: A Nambu–Jona–Lasinio model case study. *Phys. Rev. D* **2013**, *88*, 085001. [CrossRef]
178. Shahrbaf, M.; Blaschke, D.; Grunfeld, A.G.; Moshfegh, H.R. First-order phase transition from hypernuclear matter to deconfined quark matter obeying new constraints from compact stars. *Phys. Rev. C* **2020**, *101*, 025807. [CrossRef]
179. Shahrbaf, M.; Blaschke, K.S. Mixed phase transition from hypernuclear matter to deconfined quark matter fulfilling mass-radius constraints of neutron stars. *J. Phys. G Nucl. Part. Phys.* **2020**, *47*, 115201. [CrossRef]
180. Drago, A.; Lavagno, A.; Pagliara, G.; Pigato, D. The scenario of two families of compact stars. Part 1. Equations of state, mass-radius relations and binary systems. *Eur. Phys. J. A* **2016**, *52*, 40. [CrossRef]
181. Drago, A.; Lavagno, A.; Pagliara, G.; Pigato, D. The scenario of two families of compact stars. Part 2: Transition from hadronic to quark matter and explosive phenomena. *Eur. Phys. J. A* **2016**, *52*, 41. [CrossRef]
182. Wiringa, R.B.; Stoks, V.G.J.; Schiavilla, R. Accurate nucleon-nucleon potential with charge-independence breaking. *Phys. Rev. C* **1995**, *51*, 38. [CrossRef] [PubMed]
183. Isaka, M.; Yamamoto, Y.; Rijken, T.A. Effects of a hyperonic many-body force on B_Λ values of hypernuclei. *Phys. Rev. C* **2017**, *95*, 044308. [CrossRef]
184. Masuda, K.; Hatsuda, T.; Takatsuka, T. Hadron-quark crossover and massive hybrid stars with strangeness. *Astrophys. J.* **2013**, *764*, 12. [CrossRef]
185. Masuda, K.; Hatsuda, T.; Takatsuka, T. Hadron-quark crossover and massive hybrid stars. *Prog. Theor. Exp. Phys.* **2013**, *7*, 073D01.
186. Drago, A.; Lavagno, A.; Pagliara, G.; Pigato, D. Early appearance of Δ isobars in neutron stars. *Phys. Rev. C* **2014**, *90*, 065809. [CrossRef]
187. Ribes, P.; Ramos, A.; Tolós, L.; Gonzalez–Boquera, C.; Centelles, M. Interplay between Δ particles and hyperons in neutron stars. *Astrophys. J.* **2019**, *883*, 168. [CrossRef]
188. Kaplan, D.B.; Nelson, A.E. Strange goings on in dense nucleonic matter. *Phys. Lett. B* **1986**, *175*, 57–63. [CrossRef]
189. Kaplan, D.B.; Nelson, A.E. Erratum. *Phys. Lett. B* **1986**, *179*, 409.
190. Brown, G.E.; Lee, C.-H.; Rho, M.; Thorsson, V. From kaon-nuclear interactions to kaon condensation. *Nucl. Phys. A* **1994**, *567*, 937–956. [CrossRef]
191. Thorsson, V.; Prakash, M.; Lattimer, J.M. Composition, structure and evolution of neutron stars with kaon condensates. *Nucl. Phys. A* **1994**, *572*, 693–731. [CrossRef]
192. Lee, C.-H. Kaon condensation in dense stellar matter. *Phys. Rep.* **1996**, *275*, 255–341. [CrossRef]
193. Glendenning, N.K.; Schaffner-Bielich, J. Kaon condensation and dynamical nucleons in neutron stars. *Phys. Rev. Lett.* **1998** *81*, 4564. [CrossRef]
194. Keil, W.; Janka, H.-T. Hadronic phase transitions at supranuclear densities and the delayed collapse of newly formed neutron stars. *Astron. Astrophys.* **1996**, *296*, 145.
195. Bombaci, I. The maximum mass of a neutron star. *Astron. Astrophys.* **1996** *305*, 871.
196. Prakash, M.; Bombaci, I.; Prakash, M.; Ellis, P.J.; Knorren, R.; Lattimer, J.M. Composition and structure of proto-neutron stars. *Phys. Rep.* **1997**, *280*, 1–77. [CrossRef]
197. Vidaña, I.; Bombaci, I.; Polls, A.; Ramos, A. Microscopic study of neutrino trapping in hyperon stars. *Astron. Astrophys.* **2003**, *399*, 687–693. [CrossRef]

198. Burgio, G.F.; Schulze, H.-J.; Li, A. Hyperon stars at finite temperature in the Brueckner theory. *Phys. Rev. C* **2011**, *83*, 025804. [CrossRef]
199. Lattimer, J.M.; Pethick, C.J.; Prakash, M.; Haensel, P. Direct URCA process in neutron stars. *Phys. Rev. Lett.* **1991**, *66*, 2701. [CrossRef]
200. Balberg, S.; Barnea, N. S-wave pairing of Λ hyperons in dense matter. *Phys. Rev. C* **1998**, *57*, 409. [CrossRef]
201. Takatsuka, T.; Tamagaki, R. Superfluidity of Λ-hyperons admixed in neutron star cores. *Prog. Theor. Phys.* **1999**, *102*, 1043–1048. [CrossRef]
202. Takatsuka, T.; Nishizaki, S.; Yamamoto, Y.; Tamagaki, R. The possibility of hyperon superfluids in neutron star cores. *Prog. Theor. Phys.* **2000**, *105*, 179–184. [CrossRef]
203. Takatsuka, T.; Nishizaki, S.; Yamamoto, Y.; Tamagaki, R. Superfluidity of hyperon-mixed neutron stars. *Prog. Theor. Phys. Suppl.* **2002**, *146*, 279–288. [CrossRef]
204. Vidaña, I.; Tolós, L. Superfluidity of Σ^- hyperons in β-stable neutron star matter. *Phys. Rev. C* **2004**, *70*, 028802. [CrossRef]
205. Zhou, X.-R.; Schulze, H.-J.; Pan, F.; Drayer, J.P. Strong hyperon-nucleon pairing in neutron stars. *Phys. Rev. Lett.* **2005**, *95*, 051101. [CrossRef] [PubMed]
206. Wag, Y.N.; Shen, H. Superfluidity of Λ-hyperons in neutron stars. *Phys. Rev. C* **2010**, *81*, 025801.
207. Lindblom, L. Estimates of the maximum angular velocity of rotating neutron stars. *Astrophys. J.* **1986**, *303*, 146–153. [CrossRef]
208. Friedman, J.L.; Ipser, J.R.; Parker, L. Rapidly rotating neutron star models. *Astrophys. J.* **1986**, *304*, 115–139. [CrossRef]
209. Lindblom, L. Critical angular velocities of rotating neutron stars. *Astrophys. J.* **1995**, *438*, 265–268. [CrossRef]
210. Anderson, N. A new class of unstable modes of rotating relativistic stars. *Astrophys. J.* **1998**, *502*, 708. [CrossRef]
211. Friedman, J.L.; Morsink, S.M. Axial instability of rotating relativistic stars. *Astrophys. J.* **1998**, *502*, 714. [CrossRef]
212. Chandrasekhar, S. Solutions of two problems in the theory of gravitational radiation. *Phys. Rev. Lett.* **1970**, *24*, 611. [CrossRef]
213. Friedman, J.L.; Schutz, B.F. Lagrangian perturbation theory of non-relativistic fluids. *Astrophys. J.* **1978**, *221*, 937–957. [CrossRef]
214. Friedman, J.L.; Schutz, B.F. Secular instability of rotating Newtonian stars. *Astrophys. J.* **1978**, *222*, 281–296. [CrossRef]
215. Langer, W.D.; Cameron, A.G.W. Effects of hyperons on the vibrations of neutron stars. *Astrophys. Space Sci.* **1969**, *5*, 213–253. [CrossRef]
216. Jones, P.B. Astrophysical significance of the dissipation of turbulence in a dense baryon fluid. *Proc. R. Soc. Lond. A* **1971**, *323*, 111–125.
217. Levin, Y. Runaway heating by R-modes of neutron stars in low-mass X-ray binaries. *Astrophys. J.* **1999**, *517*, 328. [CrossRef]
218. Jones, P.B. Comment on "gravitational radiation instability in hot young neutron stars". *Phys. Rev. Lett.* **2001**, *86*, 1384. [CrossRef]
219. Jones, P.B. Bulk viscosity of neutron-star matter. *Phys. Rev. D* **2001**, *64*, 084003. [CrossRef]
220. Lindblom, L.; Owen, B.J. Effect of hyperon bulk viscosity on neutron star r-modes. *Phys. Rev. D* **2002**, *65*, 0653006. [CrossRef]
221. Haensel, P.; Levenfish, K.P.; Yakovlev, D.G. Bulk viscosity in superfluid neutron star cores. *Astron. Astrophys.* **2002**, *381*, 1080–1089. [CrossRef]
222. Van Dalen, E.N.E.; Dieperink, A.E. Bulk viscosity in neutron stars from hyperons. *Phys. Rev. C* **2004**, *69*, 025802. [CrossRef]
223. Chatterjee, D.; Bandyopadhyay, D. Effect of hyperon-hyperon interaction on bulk viscosity and r-mode instability in neutron stars. *Phys. Rev. D* **2006**, *74*, 023003. [CrossRef]
224. Bondarescu, R.; Teukolsky, S.A.; Wasserman, I. Spin evolution of accreting neutron stars: Nonlinear development of the r-mode instability. *Phys. Rev. D* **2007**, *76*, 064019. [CrossRef]
225. Chatterjee, D.; Bandyopadhyay, D. Hyperon bulk viscosity in the presence of antikaon condensate. *Astrophys. J.* **2008**, *680*, 686. [CrossRef]
226. Gusakov, M.E.; Kantor, E.M. Bulk viscosity of superfluid hyperon stars. *Phys. Rev. D* **2008**, *78*, 083006. [CrossRef]
227. Sinha, M.; Bandyopadhyay, D. Hyperon bulk viscosity in strong magnetic fields. *Phys. Rev. D* **2009**, *79*, 123001. [CrossRef]
228. Patruno, A. The accreting millisecond X-ray pulsar IGR J00291 + 5934: Evidence for a long timescale Spin evolution. *Astrophys. J.* **2010**, *722*, 909. [CrossRef]
229. Jha, T.K.; Mishra, H.; Sreekanth, V. Bulk viscosity in a hyperonic star and r-mode instability. *Phys. Rev. C* **2010**, *82*, 025803. [CrossRef]